water

MDPI

Review

Research Progress on Identification and Suppression Methods for Monitoring the Cavitation State of Centrifugal Pumps

Yu Zhu, Lin Zhou, Shuaishuai Lv *, Weidong Shi, Hongjun Ni *, Xiaoyuan Li, Chuanzhen Tao and Zhengjie Hou

School of Mechanical Engineering, Nantong University, Nantong 226019, China; zhu.y@ntu.edu.cn (Y.Z.); 2210310024@stmail.ntu.edu.cn (L.Z.); wdshi@ntu.edu.cn (W.S.); 2210310046@stmail.ntu.edu.cn (X.L.); chuanzhentao@126.com (C.T.); hangtang19870816@126.com (Z.H.)

* Correspondence: lvshuaishuai@ntu.edu.cn (S.L.); ni.hj@ntu.edu.cn (H.N.)

Abstract: Cavitation is a detrimental phenomenon in hydraulic machinery, adversely impacting its performance, inducing vibration and noise, and leading to corrosion damage of overflow components. Centrifugal pump internal cavitation will lead to severe vibration and noise, and not only will the performance of hydraulic machinery be adversely affected but the impact generated by the collapse of the vacuole will also cause damage to the impeller wall structure, seriously affecting the safety of the equipment's operation. To prevent the generation and development of internal cavitation in centrifugal pumps, to prevent the hydraulic machinery from being in a state of cavitation for a long time, to avoid the failure of the unit, and to realize the predictive maintenance of centrifugal pumps, therefore, it is of great significance to research the methods for monitoring the cavitation of hydraulic machinery and the methods for suppressing the cavitation. This paper comprehensively describes the centrifugal pump cavitation mechanism and associated hazards. It also discusses the current state of centrifugal pump cavitation monitoring methods, including commonly used approaches such as the flow-head method, high-speed photography, pressure pulsation method, acoustic emission method, and vibration method. A comparative analysis of these methods is presented. Additionally, the paper explores signal characterization methods for centrifugal pump cavitation, including time-domain feature extraction, frequency-domain feature extraction, and time–frequency-domain feature extraction. The current research status is elaborated upon. Moreover, the paper presents methods to mitigate cavitation and prevent its occurrence. Finally, it summarizes the ongoing research on identifying and determining the cavitation state in centrifugal pumps and offers insights into future research directions.

Keywords: centrifugal pump; monitoring method; feature extraction; cavitation state identification; cavitation suppression

check for updates

Citation: Zhu, Y.; Zhou, L.; Lv, S.; Shi, W.; Ni, H.; Li, X.; Tao, C.; Hou, Z. Research Progress on Identification and Suppression Methods for Monitoring the Cavitation State of Centrifugal Pumps. *Water* **2024**, *16*, 52. https://doi.org/10.3390/w16010052

Academic Editor: Giuseppe Pezzinga

Received: 17 November 2023
Revised: 17 December 2023
Accepted: 19 December 2023
Published: 22 December 2023

Copyright: © 2023 by the authors. Licensee MDPI, Basel, Switzerland. This article is an open access article distributed under the terms and conditions of the Creative Commons Attribution (CC BY) license (https://creativecommons.org/licenses/by/4.0/).

1. Introduction

Pumps are widely used in various fields, including national defense, industry, agriculture, drainage, and firefighting, serving as crucial components of liquid transmission systems [1]. Cavitation in centrifugal pumps not only reduces the pump's head and efficiency but also causes damage to overflow components, significantly compromising the equipment's reliability and service life. Additionally, the vibration and noise associated with cavitation can negatively impact the acoustic stealth performance of defense equipment. Volumetric pumps are usually the noisiest components of power transmission systems, where cavitation is one of the main causes of noise in hydraulic components and systems [2]. In pump devices, cavitation is most likely to occur in the inlet pipe area of the pump body. This phenomenon is often further exacerbated by the increase in localized fluid resistance caused by the use of angular joints in the inlet pipework of the pump. This situation is accompanied by complex liquid flow phenomena in the field of hydrodynamics and also determines the process for the generation and development of

cavitation phenomena inside the pump [3]. While some progress has been made through the rational design of overflow components and increasing inlet pressure to inhibit cavitation generation, complete elimination of cavitation remains challenging [4]. Consequently, addressing the cavitation problem presents a significant technical challenge in the realm of engineering applications.

The identification of the cavitation state presents several challenges that need resolution:

(1) The cavitation signal exhibits complexity, coupling, and uncertainty. The traditional energy method relies on a 3% centrifugal pump head drop as the basis for determining the initial occurrence of cavitation. However, this method suffers from significant hysteresis. Thus, it is crucial to establish the sensitivity of the centrifugal pump cavitation monitoring signals and identify values with higher sensitivity.
(2) Differentiating between various cavitation states is challenging. Establishing an accurate threshold based on the mapping relationship between the cavitation states and eigenvalues proves difficult. Moreover, changes in working conditions or pump faults lead to variations in eigenvalues such as the head, sound level, and vibration level. Relying on a single eigenvalue to set the thresholds for cavitation identification can lead to miscalculations, posing significant challenges regarding feature extraction for the centrifugal pump's cavitation state and pattern recognition.
(3) Sensor monitoring data are susceptible to unpredictable perturbations due to environmental changes or external excitation. Sudden changes or missing raw data are unavoidable, necessitating robust anti-interference measures in the cavitation state identification method.
(4) Cavitation in centrifugal pumps often coincides with other faults. Distinguishing between phenomena caused by a single fault or multiple concurrent faults poses another difficulty in the research.

The investigation of monitoring and identifying the cavitation state in centrifugal pumps not only facilitates predictive maintenance through condition monitoring but also enhances the operational efficiency and reliability of these pumps. Additionally, it offers valuable technical support and abundant engineering application data for exploring fault state identification methods in other hydraulic machinery.

2. Centrifugal Pump Cavitation Mechanism and Harm

2.1. Cavitation Mechanism

Cavitation, a highly intricate flow phenomenon unique to liquids, can be explained by two main theories: the "nucleus of cavitation" and the "saturated vapor pressure" theories. It involves a process where pressure reduction induces a partial transition of the liquid into a vapor state [5]. Combining these theories, a widely accepted definition of cavitation emerges: it occurs when the local pressure in the liquid falls below the saturation vapor pressure corresponding to a specific temperature. As a result, cavitation nuclei within the liquid rapidly grow, forming vacuoles of a certain size. These vacuoles then move to high-pressure regions, where they experience contraction, rebound, and collapse due to the surrounding fluid. The occurrence, development, pulsation, and collapse of such vacuoles, along with their accompanying complex phenomena, constitute the phenomenon known as cavitation [6].

Cavitation in centrifugal pumps primarily manifests as vane leading-edge cavitation [7], which is also the main type responsible for pump performance degradation and cavitation damage [8]. The initiation of vane leading-edge cavitation occurs at the inlet side of the vane, starting with wandering vacuole cavitation due to pressure reduction and gradually transitioning into attached cavitation [9]. Figure 1 illustrates the cavitation patterns in a centrifugal pump. The cavitation process can be categorized into three stages during the reduction of the pump's inlet pressure [10].

(1) Incipient Stage: In this stage, cavitation bubbles form and collapse in the blade inlet region, causing pitting damage to the blade [11].

(2) Weak Cavitation Stage: This stage encompasses the development of cavitation from its incipient state to the point of unstable cavitation occurrence [12]. Prolonged operation in a state of weak cavitation leads to surface damage in the overflow components, with the damage initiating on the blade inlet side and correlating with the length of the cavitation hole [11]. The scope of the weak cavitation stage can be determined through the analysis of the non-stationary dynamic properties.

(3) Unstable Cavitation Stage: In this stage, the length of the cavitation zone reaches 65% of the width of the impeller channel, leading to alternating foliar cavitation on the working surface and back of the pump blade [13]. This type of instationary flow is characterized by interference between the leading edges of neighboring blades during cavitation instability [14].

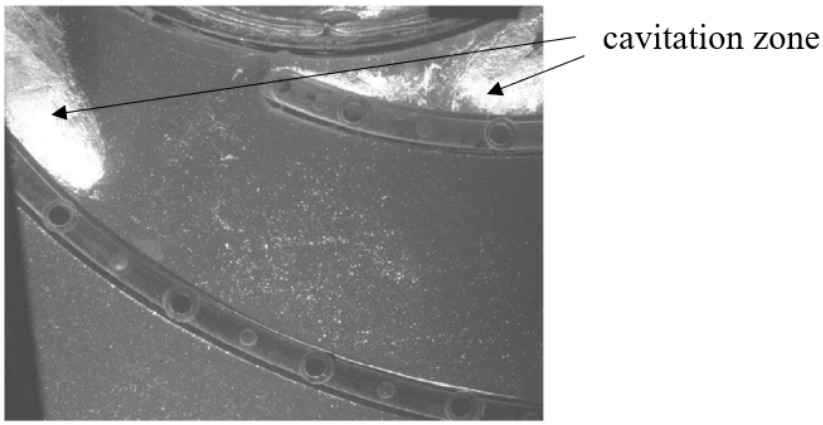


Figure 1. Cavitation pattern in a centrifugal pump [15].

2.2. Cavitation Pattern

Cavitation in hydraulic machinery can manifest in various forms, which are typically classified based on the physical properties and location within the machinery [16]. Based on the physical properties, cavitation can take on different forms, including wandering vacuoles, adherent cavitation, and vortex cavitation [6], as illustrated in Figure 2. Wandering vacuoles occur in flow fields with low-pressure points or vortex centers, moving toward high-pressure regions before collapsing, resulting in pressure pulsations. Attached cavitation, also known as fixed cavitation, involves the formation of cavities attached to solid boundaries within the flow channel [16]. It is a common type of cavitation observed in pumps and other hydraulic machinery. Due to the distinct hydrodynamic conditions, attached cavities can exhibit either relatively stable flaky cavitation or cloudy cavitation with strong instability characteristics [17]. Flaky cavitation induces small and weak pulsations, presenting a lower cavitation risk. On the other hand, cloudy cavitation displays strong instability, leading to intense cavity oscillations, making it an aggressive form of cavitation. When cloudy cavitation occurs in centrifugal pumps, it causes abnormal mechanical changes and severe cavitation effects. Additionally, attached cavitation can be further classified into two types: partial cavitation, where cavitation collapses on the surface of the airfoil or leaf sand, and supercavitation, where cavitation extends downstream of the outlet side of the airfoil or leaf sand. Various forms of attached cavitation are depicted in Figure 3. Vortex cavitation occurs when low pressure in the vortex core region experiences strong shear in the flow field. This type of cavitation has a longer duration due to the formation of vortices, which prolongs the cavities' lifetime and results in a slower collapse rate.

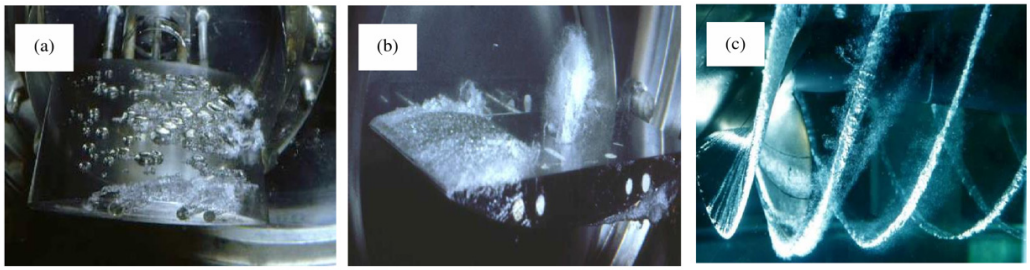


Figure 2. Several common types of cavitation [6]: (**a**) wandering vacuoles, (**b**) adherent cavitation, and (**c**) vortex cavitation.

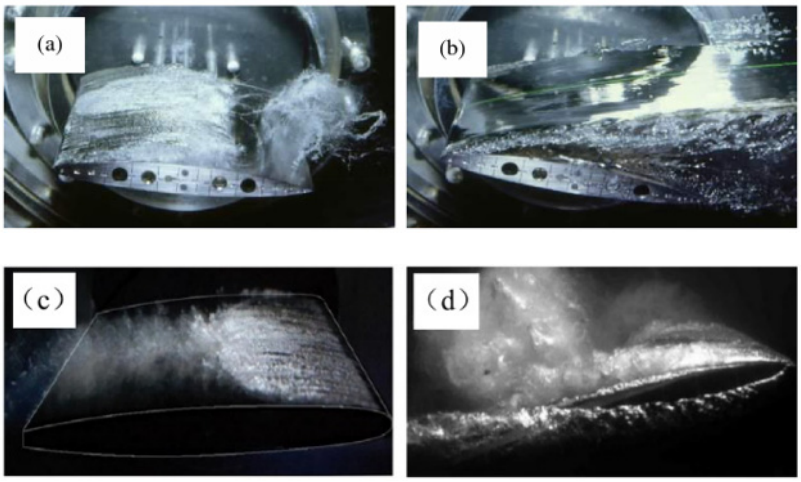


Figure 3. Common forms of attached cavities [6]: (**a**) partial cavitation, (**b**) supercavitation, (**c**) flaky cavitation, and (**d**) cloudy cavitation.

2.3. Cavitation Hazard

Over the years, both domestic and international scholars have extensively researched the underlying causes of cavitation, encompassing mechanical, thermodynamic, electrochemical, and chemical corrosion theories [18]. Among these, mechanical theory garners the most recognition [18]. This theory postulates that the collapse of vacuoles generates numerous micro-jets and shock waves, exerting a strong impact force on the overflow components' surface, leading to damage [19]. Hammitt, F.G. [20] conducted a study demonstrating that during vacuole collapse, micro-jet impulse velocities can reach up to 600 m/s, with impacts occurring at a rate of up to 1000 times per square centimeter per second, resulting in pressures as high as 705 MPa on the surface. Although the micro-jet action time is brief, lasting only a few microseconds, the repeated high-speed and high-intensity impacts can cause damage to solid surfaces, as shown in Figure 4, where cavitation damage to the blade is evident. Thus, effective monitoring and inhibition of pump cavitation development hold great significance in avoiding pump operation under cavitation conditions, thereby enhancing the pump's service life and ensuring the safe and stable operation of the unit.

Regardless of the form of cavitation, severe cavitation conditions can lead to serious consequences in a remarkably short period [22]. The hazards stemming from cavitation primarily manifest in three aspects:

(1) Performance Degradation: Cavitation disrupts the medium's continuity, resulting in a decline in the centrifugal pump head and efficiency. This leads to elevated power consumption and, in severe cases, may cause head breakage, significantly affecting the pump's overall performance.
(2) Mechanical Damage: Cavitation bubbles, upon reaching high-pressure regions, undergo collapse, releasing shock waves and micro-jets. The impingement of these on

solid surfaces causes permanent damage, a phenomenon referred to as cavitation erosion. The occurrence of cavitation severely compromises the operational safety and reliability of centrifugal pumps.

(3) Vibration and Noise: The continuous collapse of numerous vacuoles generates strong water shocks, leading to vibration and noise issues [23].



Figure 4. Impeller blades damaged by cavitation [21].

Addressing cavitation is of utmost importance to safeguarding the efficiency, reliability, and longevity of centrifugal pumps.

3. Centrifugal Pump Design Method and Numerical Calculation of Cavitation Flow

3.1. Design Methods for Centrifugal Pumps

In the process of centrifugal pump hydraulic model design optimization, the rotor and the worm casing, as very important over-flow components of the centrifugal pump, have a great influence on the external characteristics and the internal flow field state of the centrifugal pump via the reasonable selection of their geometrical parameters. Therefore, a good hydraulic model design method is crucial in the optimization process for centrifugal pumps. In the actual engineering application, centrifugal pumps generally use the design method of a one-dimensional flow model. This method in the centrifugal pump in the past design has accumulated a lot of design experience, and the theory is relatively mature, which in the actual engineering application has also had a certain effect on verification. The following are a few commonly used centrifugal pump hydraulic model design methods.

3.1.1. Modeling Approach

The model design method is a method based on similarity theory and design experience, which is based on Euler's equations, assuming that the centrifugal pumps to be optimized are geometrically and dynamically similar to the prototype pumps so that the specific speeds (ns) of the models before and after the design need to be equal.

The model design method is simple and reliable, using the principle of similarity, but the performance of the model pump is dependent on the prototype pump. If the structure of the two pumps is too different, this design method cannot be the best choice.

3.1.2. Deformation Design Method

The deformation design method is a kind of deformation of the model design method, which is based on an existing model pump, through the modification of the hydraulic model parameters of the model pump, to achieve the optimization of the target parameters and obtain the required performance index. The modified parameters are mainly:

(1) Modification of the diameter or shape of the water pipe to change the characteristics of the inlet flow;

(2) Modification of the outer diameter of the rotor blades, the blade import and export angle blade wrap angle, and the number of blades to change the head of the pump;
(3) Modification of the width of the front and back covers of the rotor and the thickness of the rotor to change the distribution of the flow characteristics of the internal flow field;
(4) The worm shell of the outlet pipe, the tongue part of the modification, to change the internal flow characteristics of the worm shell.

Although this method is relatively simple and can simply improve the performance level of the original model pump, the new model for optimization and improvement is the most used. However, this approach is more dependent on the structure of the original model pump, and its different structural parameters for different effects on the performance of centrifugal pumps, to carry out the hydraulic model design of centrifugal pumps.

3.1.3. Design Factor Method

The design coefficient method is still based on a similar theory, although the first two design methods are different from the design method due to the specific speed ns to design the runner, according to the object being no longer a specific pump but a series of good-performance pumps based on the use of statistical coefficients for the method of calculating the dimensions of the overflow components, from the new design of the pump rotor.

Although the design coefficient method is simple, the design of the product can also meet the design needs, but with the design coefficient method of the design of the runner parameters, there is a certain degree of arbitrariness, sometimes resulting in the design of the operating point and the optimal operating point not coinciding with the phenomenon, so the use of the design coefficient method of design for the product should be combined with the model test and constant optimization of the model to design a better product.

3.2. Numerical Simulation of Cavitation Flow

The research methods concerning centrifugal pump cavitation mainly include theoretical analysis, experimental research, and numerical simulation. Its advantages and drawbacks are shown in Table 1. Theoretical analysis is based on the basic theories of fluid mechanics, gas mechanics, and other basic theories, through mathematical equations and models to deduce and predict the occurrence of centrifugal pump cavitation mechanism and characteristics. Commonly used analysis methods include the cavitation number, NPSH (Net Positive Suction Head), probability of cavitation occurrence, etc. Experimental research collects data on the cavitation behavior of centrifugal pumps under different operating conditions, such as the cavitation starting point, cavitation rate, performance curves, etc., through actual laboratory or field tests [24]. Numerical calculation (CFD, Computational Fluid Dynamics) is an engineering research method based on the computer, using computer technology and showing the combination of flow, heat transfer, multiphase flow, combustion, and other phenomena in engineering, to solve a variety of complex problems in fluid dynamics, so that to a certain extent they can be predicted on the model. Due to the high-speed rotation of the centrifugal pump impeller and its twisted blade shape, the internal flow of the pump is extremely complex, which means the theoretical analysis and experimental research are often limited by the numerical calculations (CFD, Computational Fluid Dynamics) used to solve the complex flow problem, which has become an important means of researching pumps and other hydraulic machinery. In recent years, several researchers have employed various powerful mathematical techniques, such as the modified discrete fractional order Gronwall inequality, backward Euler (BE) alternating direction implicit (ADI) method as well as the discrete energy method and Cholesky decomposition method, to improve the stability and convergence of numerical methods for fluid flow problems [25–28]. Currently, numerical computation is widely used in fluid dynamics; however, researchers emphasize that the accuracy of the numerical model is crucial for the study [29]. Some scholars have proposed a predictor–corrector compact difference scheme for a nonlinear fractional differential equation. The application of the predictor–corrector

method provides both high accuracy and numerical stability in the study of complex fluid dynamics problems [30].

Table 1. Advantages and disadvantages of research methods concerning cavitation in centrifugal pumps.

Research Methodology	Advantages	Drawbacks
Theoretical analysis	(1) Low computational cost and fast results.	(1) Can only provide qualitative or approximate results; (2) Difficulty in considering complex flow changes.
Pilot studies	(1) The ability to provide authentic and reliable experimental data; (2) The ability to verify the accuracy of theoretical analyses with a high degree of confidence.	(1) Time and resource consuming; (2) Not applicable to large-scale parameter changes; (3) Inability to directly observe internal flow field changes.
Numerical calculations (CFD)	(1) The ability to accurately predict a series of performance parameters, such as the cavitation flow, pressure, velocity, etc., of hydraulic machinery such as pumps and capture flow details in the flow field; (2) Fulfilment of research tasks that are difficult to achieve via experimental testing under extreme conditions; (3) Shorten the research and development time for hydro-mechanical products and save the research and development costs [31].	(1) High-performance computing equipment is required, and parameter settings and model selection affect simulation results; (2) The need to verify the consistency of the simulation results with the actual situation.

3.2.1. Cavitation Models

For the numerical calculation of cavitation (CFD) to understand the cavitation law and to prevent its occurrence, the cavitation model is crucial to the calculation accuracy. Currently, cavitation models are mainly divided into the interface tracking method, two-fluid method, and homogeneous advection method. According to the equilibrium flow method, cavitation models can be divided into the equations of state-based cavitation models and transport equation-based cavitation models. Most of the most widely used models in the current scientific research are based on the Rayleigh–Plesset cavitation model [32,33]. The Singhal model [34], the Schnerr and Sauer model [35], and the Zwart cavitation model [17,36] are the most commonly used and representative models, and the Singhal model is based on the "full cavitation model", which takes into account the incompressible vapor and the pressure pulsation caused by turbulence energy. The effect of the pressure pulsation caused by incompressible vapor and turbulence energy on cavitation is taken into account. The model is more stable in numerical calculations, widely used, commonly used in the calculation of complex bubble flow, and also plays a large role in the field of fluid mechanics. In the Schnerr–Sauer model of water–steam mixture as a mixture containing a large number of spherical vapor bubbles, the net mass transfer rate of the vapor–liquid is the expression of the change in the volume fraction of the term. The rate of change versus the radius growth rate is used to define the interphase mass transfer rate per unit volume, with a correction for the gas volume fraction in the evaporation term. Since the model contains a large number of empirical parameters, it is suitable for numerical calculations in most cavitation flow situations.

3.2.2. Turbulence Modeling

Generally, both liquids and gases are capable of being compressed, and in scientific research, the malefactors are distinguished between compressible and incompressible fluids based on whether the density of the fluid varies or not. There are two flow states of fluids, one is laminar flow and the other is turbulent flow. Generally, the critical Reynolds number is considered to be the judgement standard for the transition of fluid flow from laminar

to turbulent, and the value of the critical Reynolds number is generally Re = 2300~4000. Turbulence is a kind of multiscale, non-constant, and complex flow field. The fluid in the cavitation flow is regarded as a homogeneous two-phase mixture, and the liquid and gas phases adopt the same form of continuity equation and momentum equation. The liquid volume fraction transfer equation is used for phase change processes in the flow field. The cavitation flow is a typical turbulent flow, and due to the complexity of turbulence, turbulence experiments are often unable to capture effective details of the flow field, so numerical simulation is currently an important means of studying turbulence. The common turbulence simulation methods at this stage are the Direct Numerical Simulation (DNS), Large Eddy Simulation (LES), and Reynolds-Averaged Navier–Stokes (RANS) methods.

The DNS method is the most direct and effective method for studying the turbulence mechanism, which is based on the principle of solving the N–S equations directly and can obtain the flow field information at any scale. Compared with the LES and RANS, the DNS method does not need to introduce any hypothetical model to close the N–S equations, and theoretically, it can solve all the turbulence problems and obtain the detailed flow field structure. However, due to the limitations of the current computational conditions, it is still unable to calculate high Reynolds number flows and complex flows. The fundamental solution to the turbulence problem is to solve the N–S equations, and at this stage, the computer conditions have not been able to meet the arithmetic power required for the DNS calculations, so the approximation of the N–S equations is the optimal solution now.

The LES method is to filter the Navier–Stokes equations (N–S equations) and then add the sublattice model for closure, which is calculated by solving the sublattice model. The LES retains the information of the small-scale flow field and greatly reduces the computational burden, which is expected to be the key to solving the turbulence problems. However, the commonly used Smargorinsky model, dynamical model, and gradient model are based on the equilibrium assumption and contain some empirical constants, so there are problems such as the low computational accuracy in the calculation process, which makes it difficult to meet the practical needs.

The RANS method is a systematic averaging of the N–S equations, followed by the inclusion of a turbulence model for closure, which is calculated by solving the turbulence model. The RANS method divides physical quantities into averaged and pulsating quantities and performs a systematic averaging of the flow field, and the Reynolds stress term generated during the averaging process is added to the turbulence model for the closure of the equations. At present, the RANS can have good convergence and accuracy at the highest possible computational accuracy, and the RANS is the main computational method for solving engineering practice problems, taking into account the operability, economy, and effectiveness of engineering practice. According to the different assumptions and treatments of stress, turbulence models can be attributed to two major types: the Reynolds stress model and the eddy–viscosity model, of which the eddy–viscosity model is more widely used. The eddy–viscosity model can be divided into the zero-equation, one-equation, and two-equation turbulence models. The two-equation model is the most popular turbulence model and the most widely used turbulence model. Low Reynolds number turbulence models are much less developed and applied than high Reynolds number turbulence models. Based on the standard k-ε model, scholars have developed the k-ω model and the SST model. The k-ω turbulence model is a two-equation empirical model that has been more commonly used in recent years. In addition, although the k-ε model has been widely used in engineering practice because the k-ω model has less computational volume compared to the k-ε model, the boundary condition processing is simple, and it can also adapt to the rougher initial turbulent flow field conditions, meaning the k-ω model is preferred for solving compressible turbulent flows.

In terms of the current situation, whether it is the common commercial software on the market or the CFD software researched by various research institutes and model units, it generally adopts the finite volume framework, and the spatial discretization accuracy is generally only of second-order accuracy. Fluent is a more mature and perfect CFD software,

which has very good simulation ability in compressible and incompressible flow, laminar flow, and turbulence problems. Fluent is a mature and perfect CFD software that has very good simulation capability for compressible and incompressible flow, laminar flow, and turbulence problems, and its solvers include a pressure-based solver and a density-based solver. The pressure-based solver has a wide range of applications, the most applications, and meets most of the multiphase flow calculations, but it cannot be used for Euler flow calculations. The pressure-based solver is the key to solving the pressure field, to make the given pressure field meet the continuity of the equation, and to carry out the pressure correction, the SIMPLE algorithm is the pressure correction method considered the most basic method. A SIMPLE algorithm is used to solve the momentum equation in turn. A SIMPLE algorithm is used to solve the momentum equation, pressure correction value equation, energy equation, component equation, and other scalar equations sequentially. The density-based solver, on the other hand, solves the momentum, continuity, energy, and component equations simultaneously, and then it solves the scalar equations, but it does not solve the pressure modifier equation because the pressure is obtained from the equation of state. The density-based solver is suitable for flows with strong coupling between the density, energy, momentum, and components due to strong bulk forces, such as high-speed compressible flows, supersonic flows, and surge interference problems.

Currently, the RANS is the mainstream model for calculating turbulent flow. However, these models oversimplify the physical nature of turbulent flow and heat transfer and lose important first-order turbulent pulsation information, so some scholars have proposed a method based on the partial averaging of turbulent pulsation quantities. Unlike the traditional statistical averaging method, this method uses a group averaging method (partial averaging) for the turbulent pulsation velocity. In addition, with the continuous development of artificial intelligence, machine learning (Machine Learning, ML) and deep learning (Deep Learning, DL) have become research hotspots in various industries. In the face of the massive data generated by turbulence experiments and numerical simulation of turbulence, ML's and DL's powerful data processing capabilities provide favorable conditions for the combination of fluid dynamics and artificial intelligence, making them a new solution to fluid problems. Through the machine learning method, it is possible to improve the existing fluid mechanics theory, and to improve or replace the existing turbulence model and sub-grid scale (SGS) model, so that it can be accurately and efficiently applied in engineering practice. Machine learning in fluid mechanics turbulence model research mainly has modeled uncertainty analysis, improving the existing turbulence model and replacing the traditional turbulence model in these three directions.

4. Current State of Research on Monitoring Methods for Centrifugal Pump Cavitation

Various methods are commonly employed for monitoring cavitation in centrifugal pumps, such as the flow-head method, high-speed photography, pressure pulsation method, acoustic emission method, and vibration method [37].

4.1. Flow-Head Method

The flow-head method, a traditional approach for determining cavitation in centrifugal pumps, involves identifying the initial cavitation point as a 3% head reduction from the critical point. However, this method exhibits clear hysteresis, as it fails to detect the early stage of cavitation effectively. By the time the head decreases by 3%, the pump's internal cavitation may have already progressed to a severe extent, leading to significant degradation in the pump's efficiency and performance. Xu et al. [38] conducted a statistical analysis of the parameter changes throughout the cavitation stage in centrifugal pumps and highlighted the limitations of defining the beginning of cavitation solely based on the 3% head reduction. They observed that during the initial cavitation stage, the parameter changes are minimal, and the performance curve exhibits a steep decline when reaching the severe cavitation stage. Subsequently, Wu et al. [39] conducted experimental research involving the continuous start-stop process in transient pump operation. They measured

performance parameters, including transient speed, head, flow, and suction pressure, and analyzed the impact of cavitation on the transient hydrodynamic performance of the centrifugal pump during operation.

4.2. High-Speed Photography

High-speed photography proves to be a direct and effective method for capturing the cavitation phenomenon that characterizes cavitation generation, making it the most reliable means of identifying the cavitation state. Gerkula et al. [40] conducted high-speed photography of a rotary paddle turbine within a cavitation water hole, revealing flaky cavitation bubbles at the guiding edge region of its blade, along with numerous cavitation bubbles captured at the blade's root. Wang et al. [41] analyzed the results of high-speed photographic tests with different cavitation phases under three operating conditions: 0.8 Q_d, 1.0 Q_d, and 1.2 Q_d (Q_d—rated flow rate). Figure 5 shows the results of high-speed photography tests with different cavitation numbers under different working conditions, and compared with the cavitation performance test, it is found that when the cavitation coefficient of the rated working condition 1.0 Q_d is 0.94 and 0.538, there are no obvious cavitation bubbles in the whole runner, while when the cavitation coefficient is reduced to 0.478, it can be seen that a small number of cavitation bubbles appeared in the impeller runner, and the bubbles did not appear on each blade, which is mainly due to the asymmetry of the worm shell structure and the effect of the pressure pulsation generated at the spacer tongue, which can be defined as the traditional cavitation incipient point at this time. Therefore, the incipient point of the cavitation stage σ = 0.478 is judged according to the high-speed photography, which is earlier than the critical point of the cavitation incipient judged according to the head drop of 3%. As the inlet pressure continues to decrease, the cavitation number continues to decrease to 0.472, and cavitation bubbles appear on each rotating blade.

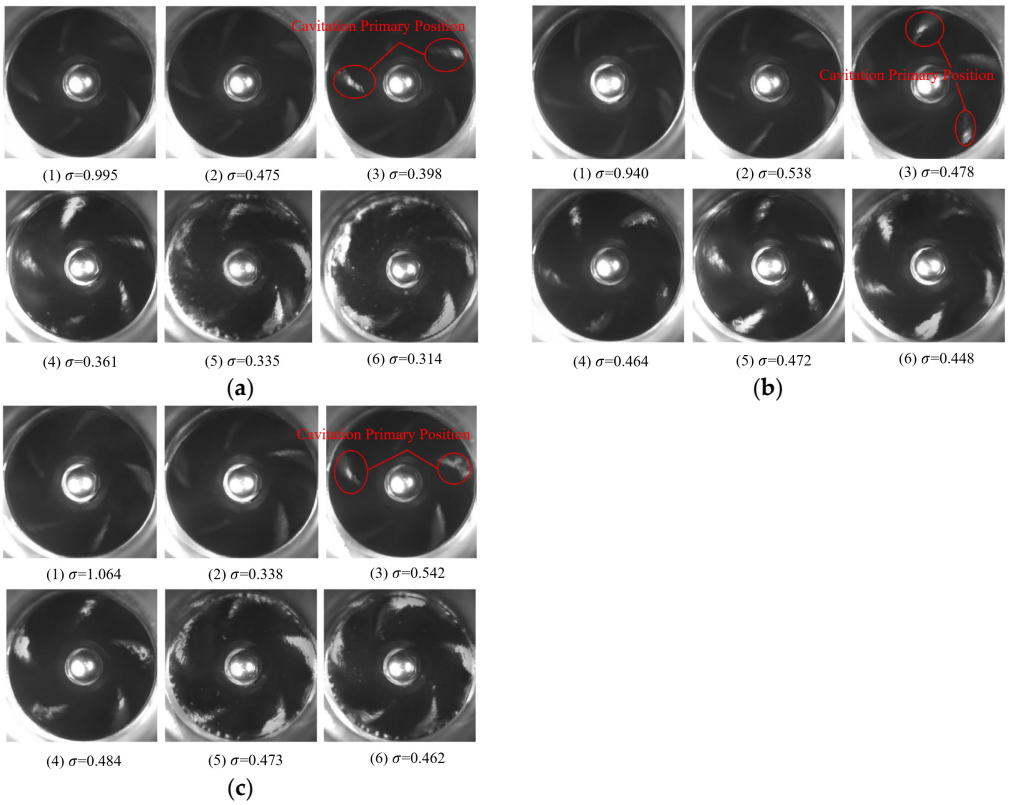


Figure 5. Experimental results of high-speed photography with different cavitation numbers under different working conditions [41]: (**a**) 0.8 Q_d, (**b**) 1.0 Q_d, and (**c**) 1.2 Q_d.

As the inlet pressure p_{in} decreases, when cavitation starts to occur, the inlet pressure p_{in} at this particular condition corresponds to a particular value of σ, which is called the incipient cavitation number, as denoted by σ_i:

$$\sigma_i = \frac{(p_{in})_i - p_v}{0.5\rho U^2}, \quad (1)$$

Here, $(p_{in})_i$ denotes the inlet pressure at the onset of cavitation in Pa;
p_v denotes the saturation pressure of the liquid at ambient temperature in Pa;
ρ denotes the density of the liquid in kg/m^3; and
U denotes the circumferential component of the velocity at the impeller outlet in m/s.

Table 2 shows a comparison between the traditional cavitation initial point and the cavitation initial point under different flow rates, and the cavitation initial points of the high-speed photography method are all larger than the traditional cavitation initial point, which indicates that the high-speed photography method can capture the formation of bubbles in the fluid earlier and can determine the cavitation initial point earlier. Therefore, the traditional cavitation determination method has obvious hysteresis, and the cavitation initiation is determined earlier than the traditional method according to high-speed photography.

Table 2. Comparison of the conventional cavitation incipient point and the cavitation incipient point at different flow rates [41].

Flow Condition	0.8 Q_d	1.0 Q_d	1.2 Q_d
Conventional cavitation point	0.336	0.423	0.485
High-speed photography of cavitation incipient points	0.398	0.478	0.542

Researchers have employed high-speed photography to study the cavitation characteristics in various hydraulic machinery applications. Cui et al. [42] conducted a study using a combination of high-speed photography and numerical simulation to explore cavitation inside a high-speed induced wheel. The research revealed the presence of leakage vortex cavitation, lamellar cavitation, and cloud cavitation in the flow channel during the cavitation development period. Zhang et al. [43,44] utilized high-speed photography to investigate the cavitation characteristics of an axial pump during startup braking. Their findings indicated that with an increase in the rotational speed, the cavitation area on the back side of the blade gradually shifted from the central trailing edge to the trailing edge and hub direction. Kim et al. [45] focused on the influence of temperature on the cavitation characteristics of the induced wheel. By elevating the temperature of the liquid medium, they used a high-speed camera to observe the cavitation attached to the blades of the wheel at different temperatures. In another study, Shen et al. [46] employed high-speed photography to examine the mechanism of vortex cavitation at the top of the blade. They analyzed the development characteristics of the flow rate and cavitation numbers. The experiment demonstrated that incipient cavitation is more likely to occur at lower flow rates, resulting in an unstable cavitation pattern. A comparison of the pressure pulsation and the cavitation structure revealed that the lowest peripheral pressure occurred at the suction surface of the blade.

Although high-speed photography provides higher monitoring accuracy, it does have certain limitations. This method demands specific requirements for the equipment and test environment, leading to higher test costs. Consequently, high-speed photography is limited to transparent devices and specific occasions where its benefits outweigh the associated expenses.

4.3. Pressure Pulsation

Pressure pulsation signals offer valuable insights into the stage of cavitation in centrifugal pumps [47]. Guo et al. [48] established a test bench to collect pressure pulsation signals and investigated the correlation between the cavitation phenomena and pressure pulsation

in the pump. They observed that the pressure pulsation amplitude increased at the onset of cavitation, with the peak occurring at the lobe frequency. As the cavitation severity deepened, the pressure pulsation amplitude shifted toward the low-frequency band, exhibiting a broadband characteristic. Zhao et al. [49,50] analyzed the flow characteristics and pressure pulsations at the impeller inlet under cavitation conditions, studying the non-constant cavitation characteristics of centrifugal pumps with low specific rotational speeds using the Zwart–Gerber–Belamri model. The results demonstrated that the total turbulence energy of the impeller under perforated conditions was smaller than that of the original impeller, with a reduced distribution area of vapor bubbles. Studies by Wang et al. [51] on an ultra-low specific speed centrifugal pump utilized the Zwart–Gerber–Belamri model for numerical calculations and experiments. The research indicated that when cavitation occurs, it generates low-frequency and wide-frequency pressure pulsations. As cavitation develops further, the frequency domain and amplitude of the pressure pulsations exhibit specific patterns of change.

Mou et al. [52] discovered that the bubble volume and bubble area on the vane suction surface were larger than those on the pressure surface, causing flow channel blockage and vortex generation during severe cavitation. This, in turn, leads to enhanced pressure pulsation and irregular radial force distribution. With the IS80-50-250 model centrifugal pump as the object of study, centrifugal pump parameters are: flow Q = 50 m^3/h, head H = 80 m, speed n = 2900 r/min, cavitation margin NPSH = 1.8 m; inlet diameter D_1 = 80 mm, impeller for the closed impeller, the number of blades is 5, impeller outer diameter D_2 = 252 mm; calculation process conveying medium for the 25 °C water and air two-phase mixture, the medium at the temperature of the vaporization pressure pv = 3475 Pa, the mass flow rate of the imported Q_m = 13.89 kg/s, a total of six kinds of export pressure values *p* set in order of *p* = 0.81 MPa, *p* = 0.80 MPa, *p* = 0.79 MPa, *p* = 0.78 MPa, *p* = 0.77 MPa, *p* = 0.73 MPa. As can be seen from Figure 6, the head with the decline of the cavitation margin first slowly changes after a sharp decline; when the cavitation margin >4 m, the head is almost unchanged, indicating that at this time there is no cavitation phenomenon in the impeller; when the cavitation margin <1 m, the head falls sharply, the impeller channel occurs in serious cavitation, the loss of kinetic energy is greater, affecting the kinetic energy to the conversion of pressure energy. Numerical calculations show that with the cavitation margin = 0.97 m, the centrifugal pump head decreased by 3%, just in the critical cavitation margin point. A comparison of the numerical simulation with the experimental cavitation performance curve shows that there is a certain error of <3%, which meets the calculation requirements.

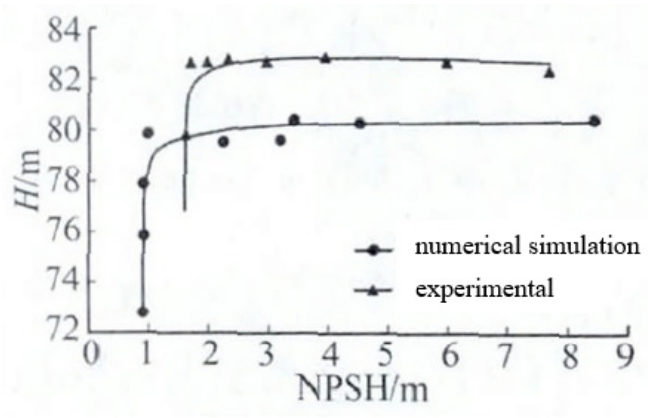


Figure 6. Cavitation performance of a centrifugal pump.

The selected six operating conditions were to analyze the internal flow field of the centrifugal pump, the parameters are shown in Table 3, and from Figure 7a, it can be seen that under the operating conditions 1 and 2, the impeller shows a weak cavitation state, a small number of bubbles appearing in the impeller inlet; under operating condition 4, the

pressure surface of the vane began to appear bubbles; and under operating condition 5, the impeller occurred in a serious cavitation, a larger bubble area and bubble volume blocked the impeller channel, causing flow separation, increasing energy loss, which in turn affects the hydraulic performance of the centrifugal pump. It is worth noting that the bubble volume and bubble area on the suction surface are usually larger, which is because the pressure on the suction surface is lower, easy to occur cavitation, and due to the dynamic and static interference of the impeller, the bubbles show asymmetric distribution. Figure 7b shows the static pressure distribution of the impeller with the change in the cavitation residual cloud diagram, the impeller is in a weak cavitation state, and the static pressure gradient changes uniformly, with the intensification of the cavitation phenomenon in the pump, the static pressure distribution of the impeller unevenly increased, the low-pressure area gradually expands, the static pressure of the impeller outlet is first slowly reduced and then rapidly reduced, indicating that the occurrence of cavitation, affecting the centrifugal pump speed to the pressure of the energy conversion process, resulting in the impeller outlet pressure decreasing, thus reducing the head. Figure 7c shows the impeller liquid flow with the distribution of the cavitation margin changes. A larger cavitation margin will lead to the impeller speed from the inlet to the outlet gradually increasing, leading to the formation of a positive velocity gradient in the impeller surface vortex; to reach the critical cavitation margin, the vortex disappeared on the vane surface vortex and appeared in the back of the vane, the impeller speed gradient shifted from positive to negative, the speed in the radius direction first increased and then decreased, and the speed in the middle of the impeller flow path reached the maximum. The velocity reached the maximum value at the middle runner of the impeller. The reason is that the bubble occupies the impeller channel so that the fluid overflow area decreases and the flow rate increases; in the bubble area after the liquid overflow area suddenly increases, the flow rate decreases. At the same time, the outlet pressure is higher than the internal pressure of the impeller, resulting in a reverse pressure gradient, so that the back of the blade boundary layer separates and the phenomenon of de-fluxing forms a vortex; the more serious the cavitation, the greater the vortex and the fluid build-up here, resulting in a greater loss of kinetic energy, which affects the performance of the pump, resulting in a decline in the head.

Numerical calculations and analysis by He et al. [53–55] showed that during different stages of cavitation development in the centrifugal pump, the main frequency of the pressure pulsation at the monitoring points in the worm shell corresponds to the blade frequency. When cavitation occurs, the maximum value of the pressure pulsation occurs near the first cross-section of the worm shell. Spectrograms demonstrate an increase in the spectral peaks of the high-frequency part and an increase in the frequency components with the development of cavitation. Yang et al. [56] studied the impact of the double worm shell structure on the cavitation flow field of the centrifugal pump. They found a significant increase in the pressure pulsation amplitude at the septum tongue under cavitation compared to non-cavitating conditions after implementing the double worm shell. Additionally, Lu et al. [57] investigated the cavitation characteristics in centrifugal pumps operating at a small flow rate, studying the pressure pulsations at the inlet and outlet of the pumps. Their findings indicated that the spacer tongue of the pump worm casing could interfere with the impeller, affecting the pump's operation. With the development of cavitation, the main frequency at the pump inlet shifted to the low frequency, while the main frequency peak at the pump outlet existed at twice the axial frequency. Lu et al. [58] studied the cavitation development process through experiments and numerical simulations, analyzing the pressure pulsation changes at the inlet and outlet of the centrifugal pump. They noted that the pressure pulsation at the pump inlet was more sensitive to cavitation changes.

Although the pressure pulsation method offers higher accuracy, precise measurements often require using the four-end network method, necessitating multiple holes to be drilled in the pipeline or pump body. This procedure can cause damage and inconvenience, limiting its application in certain situations.

Table 3. Working condition parameters [52].

Condition	p/MPa	NPSH/m
1	0.81	4.52
2	0.80	3.43
3	0.79	3.19
4	0.78	2.24
5	0.77	0.97
6	0.73	0.91

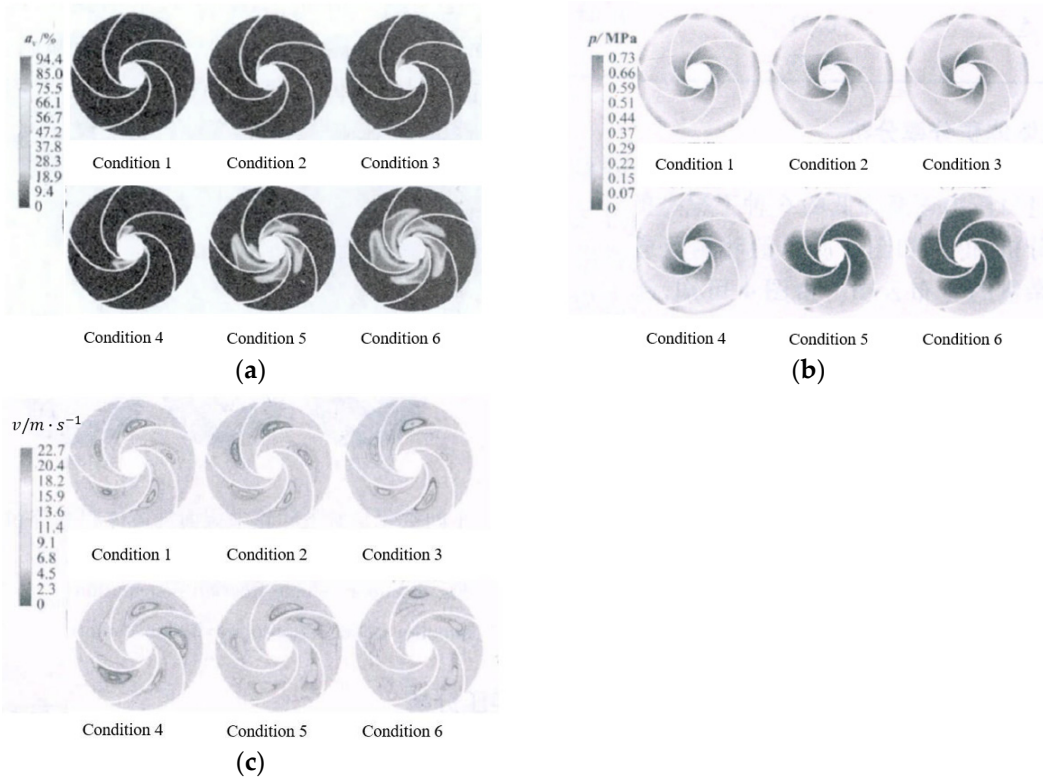


Figure 7. (**a**) Cross-sectional gas volume rate distribution cloud in the impeller with different cavitation margins, (**b**) cross-sectional static pressure distribution cloud in the impeller with different cavitation margins, and (**c**) cross-sectional streamline distribution in the impeller with different cavitation margins [52].

4.4. Acoustic Emission Method

The acoustic emission method [59] utilizes the impact force generated when cavitation vacuoles collapse in water pumps, resulting in the formation of acoustic emission waves. By measuring and analyzing the signal characteristics of these emissions, the critical point of the initial cavitation can be determined.

Liu et al. [60] sought to explore the relationship between acoustic emission signals and cavitation. They employed the wavelet method to decompose the import and export acoustic signals of different cavitation stages. It was discovered that the energy values within different frequency bands exhibited distinct changes, enabling the identification of cavitation based on these energy variations. Dong et al. [61] quantitatively analyzed liquid-loaded noise signals from centrifugal pumps under various cavitation states to determine the applicable frequency range for cavitation identification. The 3σ criterion was used to establish the cavitation threshold, with a 1% increase in the broadband sound pressure level of the liquid-loaded noise in the frequency band of 2000~3000 Hz serving as the basis for detecting incipient cavitation. Alfaye et al. [62] employed a broadband otoacoustic emission transducer to collect signals from different cavitation stages. They

observed that the peak frequency of the signal during the incipient stage of cavitation was concentrated in the frequency band of 100~300 kHz, while the severe stage of cavitation shifted to a higher frequency band of 200~700 kHz. This acoustic emission method allows for the reception of ultrasonic waves emitted by bubble collapse during the early stages of cavitation, leading to more accurate and timely judgments. However, it requires precise and expensive supporting facilities, limiting its widespread use.

4.5. Vibration Method

The vibration method is widely recognized as an effective means of identifying the cavitation state due to its simple setup, non-destructive nature, and robust anti-interference capabilities. This approach involves installing acceleration sensors directly on the pump body to collect vibration signals under various operating conditions. The acquired data are then analyzed in the time–frequency domain to extract the parameter characteristic patterns.

Su et al. [63,64] analyzed the cavitation characteristics of centrifugal pumps and addressed the issue of signal interference in extracting cavitation characteristic signals using vibration or acoustic signals under laboratory conditions. They researched methods to eliminate such interference and proposed techniques for determining the cavitation threshold. Additionally, Zhao et al. [65] defined the cavitation incipient point and the cavitation extreme point based on different methods of processing test data. They proposed a more refined and accurate cavitation stage division method compared to the traditional approach, segmenting the entire cavitation process into five stages: uncavitation stage, cavitation incipient stage, cavitation development stage, severe cavitation stage, and over-severe cavitation stage. Through processing and analysis of vibration noise and frequency spectrum data, they identified frequency bands with high sensitivity to cavitation, quantified cavitation thresholds for different measurement quantities with wide-frequency level values, and proposed cavitation determination methods based on liquid-loaded noise and solid-loaded vibration wide-frequency level values. Figures 8 and 9 depict the sound pressure level changes in different frequency bands during the liquid-loaded noise from the non-cavitation stage to the cavitation development stage and the wide-frequency vibration level changes in different frequency bands at different measurement points on the solid vibration pump body during the same stages. The maximum value of the vibration level in the 10~50 Hz band increases by about 6 dB compared to the average value in the uncavitated stage, while for the 1000~3000 Hz band, the effect of cavitation on the vibration level is slightly weaker by about 3 dB because of the higher broadband energy level. The 3σ rule is used to determine the threshold value of the solid-loaded vibration frequency band, and the average value of the solid-loaded vibration broadband vibration level data in the uncavitation stage in the 10~50 Hz band and the 1000~3000 Hz band respectively is taken as the benchmark, and the percentage of the change in the relative benchmark value is taken as the threshold data sample for processing and statistics, as shown in Table 4. At the same time, to avoid the influence of solid-loaded vibration fluctuation on the accuracy of the cavitation determination in the uncavitation stage, and at the same time, to take into account the sensitivity of cavitation determination, it is determined that the threshold value of the wide-frequency vibration level change rate of solid-loaded vibration in the frequency band of 10~50 Hz is 1.0%, and the threshold value of the broad-frequency vibration level change rate in the frequency band of 1000~3000 Hz is 1.1%. That is, when the broadband amplitude of the solid-loaded vibration in the 10~50 Hz frequency band rises by 1.0% compared with the average amplitude of the uncavitation stage, or when the threshold value of the broadband amplitude change rate in the 1000~3000 Hz frequency band is 1.1%, it is considered that cavitation occurs.

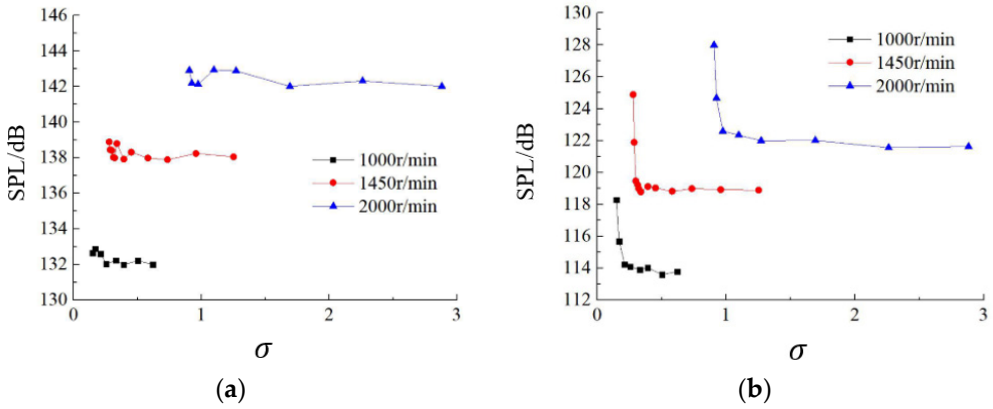


Figure 8. The variation rule of the sound pressure level from the uncavitation stage to the cavitation development stage in different frequency bands of liquid-loaded noise [65]: (**a**) 0~100 Hz bandwidth frequency sound pressure level change, and (**b**) 2000~3000 Hz bandwidth sound pressure level change.

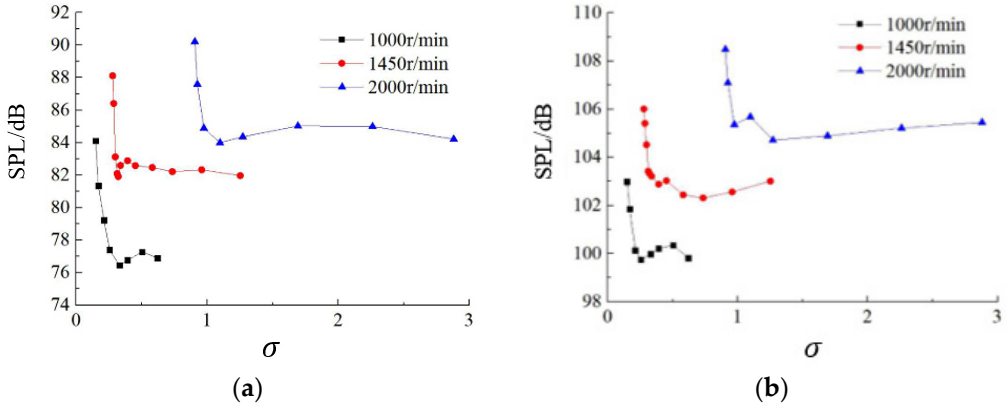


Figure 9. Wide-frequency amplitude variation rule of different frequency bands from the uncavitation stage to the cavitation development stage at the measurement point of the solid-loaded vibrating pump body [65]: (**a**) 10~50 Hz frequency band-wide frequency level change, and (**b**) 1000~3000 Hz frequency band-wide frequency level change.

Table 4. Thresholds for the rate of change of solid-load vibration under different rotational speed conditions [65].

Bandwidth/Hz	n/(r·min^{-1})	$\bar{X}_a$/(%)	S_a/(%)	Threshold/(%)
10~50	1000	2.22	0.43	0.93
	1450	1.75	0.31	0.82
	2000	1.82	0.35	0.77
1000~3000	1000	1.60	0.19	1.03
	1450	0.92	0.11	0.59
	2000	1.54	0.18	1.00

Various researchers have employed vibration-based methods to monitor cavitation in centrifugal pumps, revealing valuable insights into the cavitation development process. Zeng [66] collected vibration signals from a 150-125-315 centrifugal pump before and after cavitation occurrences at different Net Positive Suction Head available ($NPSH_a$) levels. The study demonstrated a sharp increase in the root mean square value of the acceleration at $NPSH_a$ values of less than 2.84, 2.92, and 3.45 m, establishing them as critical cavitation margins determinable through the vibration method. Cao et al. [67]

adopted a deep learning-based approach for cavitation state identification in centrifugal pumps using vibration signals from the pump casing. They constructed an improved octave band feature matrix and time–frequency feature matrix, leveraging deep-learning networks for classification. Similarly, Zhang et al. [68] investigated the vibration frequency domain features of centrifugal pump cavitation using the Smoothed Pseudo Wigner–Ville Distribution (SPWVD) transformation, observing frequency changes in the range of 160 to 200 Hz during cavitation development.

Ye et al. [69] provided insights into the cavitation flow field of centrifugal pumps at different flow rates, analyzing vacuole morphology during various stages of cavitation development and its relationship with pump vibration. The main design parameters of the test pump are the flow rate Q_d = 25 m^3/h, head H_d = 15 m, rotational speed n = 2500 r/min, and specific rotation ns = 135. To facilitate the observation of the cavitation flow in the centrifugal pump, the design of the impeller geometric parameters with a large corrosion allowance: vane inlet diameter D_1 = 100 mm, impeller outlet diameter D_2 = 170 mm, impeller export width b_2 = 6 mm, vane number Z = 6, vane inlet angle $\beta_1 = 22°$, vane outlet angle $\beta_2 = 18°$, vane wrap angle $\varphi = 90°$. 6 mm, the number of blades Z = 6, blade inlet angle $\beta_1 = 22°$, blade outlet angle $\beta_2 = 18°$, blade wrap angle $\varphi = 90°$. At the beginning of the test, as the inlet pressure decreases the head rises slightly, the pump inlet pressure at this stage of every 10 kPa decreases in the measurement of a working point. Figure 10 shows the test pump at different flow rates under the cavitation performance curve, the horizontal coordinates for the logarithmic coordinates, and the solid triangle for the small flow rate under the rotating cavitation occurs in the interval. In 1.2 Q_d, due to the cavitation mainly concentrated in the pressure surface, the head soon began to decline, and in the cavitation margin of 6.7 m, when the critical cavitation margin point (head decreased by 3%), the remaining three flow rates in the arrival of the critical cavitation margin point before the cavitation is mainly concentrated in the suction surface, the critical cavitation margin relative to the 1.2 Q_d under a significant reduction.

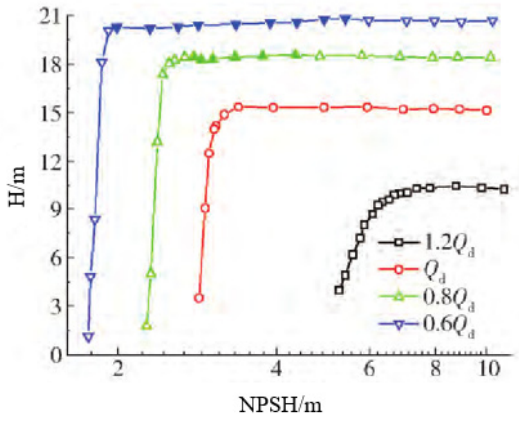


Figure 10. Cavitation performance curves at different flow rates.

Figure 11 shows the variation in the length (L_{cav}) and vibration of the vacuole cluster with the cavitation margin for the three flow conditions of 0.8 Q_d, 1.0 Q_d, and 1.2 Q_d, and the corresponding cavitation number (σ) is shown as the top horizontal coordinate. For the 0.8 Q_d case (Figure 11a), the maximum length of the vacuole cluster on the suction surface after the occurrence of rotational cavitation firstly increases rapidly and then remains essentially stable, while the minimum length first remains essentially stable and then increases rapidly, the vacuole cluster remains thin, and the scale of the dislodged vacuole cluster is small. For the 1.0 Q_d case (Figure 11b), the length of the vacuole cluster on the suction–suction surface increases steadily and remains relatively thin as the cavitation margin decreases. At the beginning of cavitation on the pressure surface, the presence of the vacuole cluster is unstable, and then the growth rate of the pressure surface vacuole cluster length and super vacuole length gradually increases. The vibration increases slowly

at the initial stage and then decreases and remains almost constant when the cavitation margin decreases to about 9 m. The vibration is also very stable at the initial stage. After cavitation occurs at the pressure surface, the vibration starts to increase, especially after supercavitation occurs, the vibration increases significantly, and the amplitude of vibration at the worm shell is also larger than that at the bearing.

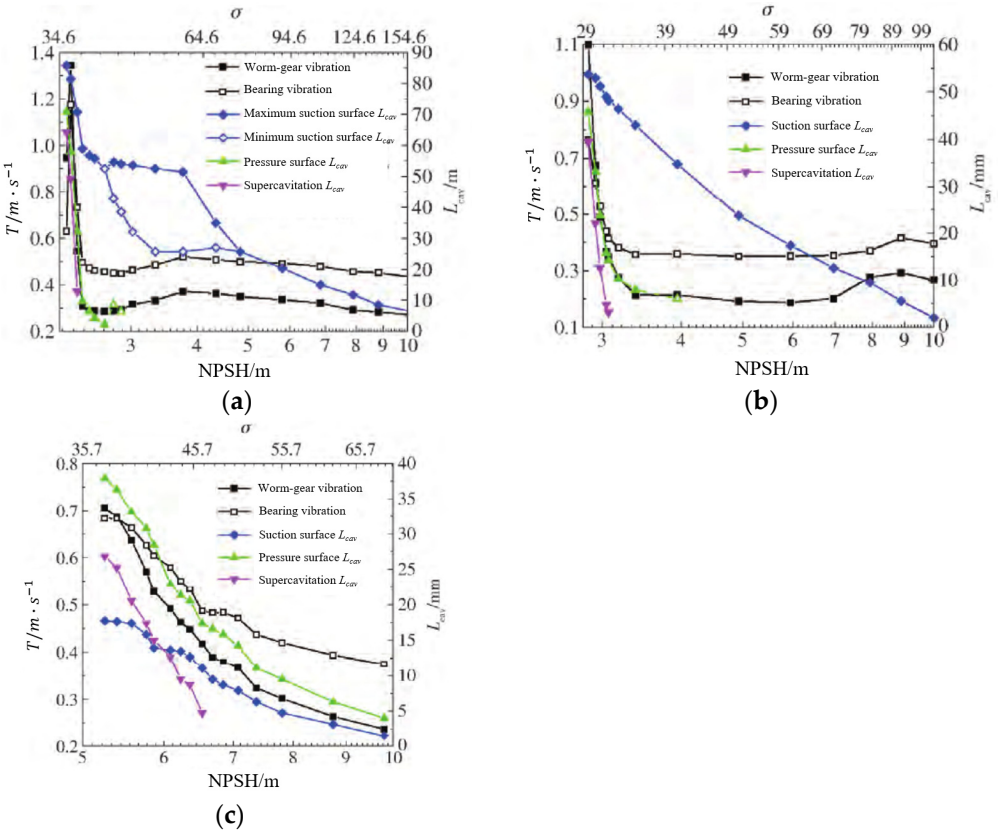


Figure 11. (**a**) Variation of vibration and L_{cav} with the cavitation margin at 0.8 Q_d, (**b**) variation of vibration and L_{cav} with the cavitation margin at 1.0 Q_d, and (**c**) variation of vibration and L_{cav} with the cavitation margin at 1.2 Q_d [69].

He et al. [70] conducted cavitation tests with two vibration acceleration sensors installed at different worm case positions, comparing multiple feature extraction methods for cavitation identification. The study revealed that the feature extraction method with improved octave frequency exhibited higher accuracy. Further research by Ye et al. [71] involved collecting centrifugal pump cavitation-induced vibration signals and employing standard deviation, skewness, and kurtosis features for support vector machine (SVM) training to propose an incipient cavitation monitoring method. Meanwhile, Farhat et al. [72] used vibration acceleration sensors to collect cavitation signals from hydraulic turbines, identifying cavitation and its severity using statistical analysis and spectral methods. Vibration signals from different cavitation stages were analyzed by Yagi et al. [73], revealing that the peak frequencies in the initial cavitation stage were concentrated at 20–30 kHz, forming the basis for cavitation occurrence judgment. Cernetic [74] monitored the pump incipient cavitation residuals through acceleration sensors and microphones, while Tomaz et al. [75] conducted an experimental study of noise and vibration in an axial-flow hydraulic turbine under cavitation using hydrophones and accelerometers, establishing consistent relationships between the cavitation numbers and vibration and noise signal curves. Lee et al. [76] acquired vibration signals to monitor the equipment state and employed wavelet analysis for fault signal analysis, leading to the development of a fault diagnostic system. Additionally, Buono et al. [77] designed a rotor pump cavitation fault diagnosis system based

on vibration signal detection using the Fast Fourier Transform (FFT). The system enabled real-time monitoring of the FFT vibration spectra, accurately predicting cavitation faults in the pump. Overall, vibration-based monitoring methods offer valuable insights into the cavitation phenomena and contribute significantly to the development of effective cavitation diagnostic systems. The advantages and drawbacks of different cavitation state identification methods are shown in Table 5.

Table 5. Comparison of the advantages and disadvantages of different cavitation state identification methods.

Monitoring Methodology	Advantages	Drawbacks
Flow-head method	(1) Simple and easy to implement.	(1) Hysteresis.
High-speed photography	(1) High monitoring accuracy; (2) Capable of capturing the state of cavitation development.	(1) Requirements for the use of objects and environmental conditions are demanding, and the cost of testing is high; (2) Only applicable to transparent model machines and rare specific occasions.
Pressure pulsation	(1) Higher precision.	(1) It is usually necessary to use the four-end network method to drill multiple holes in the pipeline or pump body, which can cause damage to the pump body or pipeline; (2) The application is not convenient.
Acoustic emission method	(1) The ultrasonic wave emitted by the bubble collapse can be received when cavitation is just generated, and the judgment is more accurate and timely.	(1) Susceptible to environmental disturbances; (2) Requires very sophisticated and expensive supporting facilities.
Vibration method	(1) Simple arrangement, without destroying the research object; (2) Strong anti-interference and high signal sensitivity.	(1) In complex environments, the location and number of monitoring points have a direct impact on the accuracy of cavitation identification; (2) It cannot meet the needs of certain remote real-time monitoring.

5. Research Status of Signal Feature Extraction Methods for Centrifugal Pump Cavitation

Dynamic sensors acquire raw signals from centrifugal pumps during various operating states over time, containing valuable transient information. Due to the vast amount of data in the raw signals, processing is required to extract the distinctive features of different cavitation states. Additionally, the extracted features often possess high dimensionality, potentially containing redundant or irrelevant information. Therefore, selecting and analyzing the most relevant features becomes crucial [78]. The commonly used feature extraction methods can be categorized into time-domain, frequency-domain, and time–frequency-domain feature extraction techniques.

5.1. Time-Domain Feature Extraction

Time-domain features analyze the waveform characteristics of the signal with time as the variable. Common methods for time domain feature extraction encompass quantitative eigenvalue extraction, such as the maximum value, mean square value, and root mean square value. Additionally, dimensionless eigenvalue extraction includes waveform indicators, peak indicators, margin indicators, craggy indicators, and pulsation indicators. Correlation analysis techniques, such as autocorrelation and intercorrelation, are also utilized. For instance, Li et al. [79] employed four statistical parameters, namely, variance, rms, rms, and probability density function (PDF), from the inlet pressure pulsation time-domain signal to identify the cavitation incipient state of centrifugal pumps under rated operating conditions. However, the identification effect was found to be poor for other operating

conditions. In a study by Duan et al. [80], vibration signals were collected from various measurement points of centrifugal pumps, and it was observed that the vibration acceleration level increased by approximately 10 dB after the occurrence of cavitation, thereby serving as a characteristic value for the judgment of cavitation.

5.2. Frequency-Domain Feature Extraction

Frequency-domain features analyze signal characteristics with frequency as the variable, offering a more concise representation compared to time-domain features, although the latter are more intuitive. Common methods for frequency-domain feature extraction include spectral analysis, envelope analysis, order ratio spectral analysis, and holographic spectral analysis, among others. In centrifugal pumps, the prevalent characteristic frequencies are the shaft frequency, lobe frequency, and multiplicative and harmonic frequencies. For example, He et al. [81] determined the occurrence of cavitation by setting an amplitude threshold at the shaft frequency of the cavitation ultrasonic signal. Qing et al. [82] employed two power bands to identify three cavitation states by plotting the average power of each frequency band of the centrifugal pump cavitation noise signal against the cavitation margin. Dong et al. [83] proposed 2000~3000 Hz as a wide frequency band suitable for judging cavitation by analyzing changes in the flow coefficient and cavitation number on the vibration noise spectrum, and they established a 94.5 dB threshold for judging cavitation in vibration signals and a 97 dB threshold for noise signals. Cudina et al. [84] suggested that the frequency of 147 Hz could be used as a basis for identifying the cavitation state, but this was not confirmed in other scholars' studies.

5.3. Time–Frequency-Domain Feature Extraction

Time–frequency-domain feature extraction enables the extraction of multiple statistical eigenvalues from the original signal in the time–frequency domain. Common methods for time–frequency-domain feature extraction include wavelet decomposition, Wigner–Ville distribution, Hilbert–Huang transform, and local mean decomposition, among others. Wang et al. [85] employed the statistical line count to plot the mode maxima of a wavelet transform and identify the main amplitude mutation points in the cavitation noise signal, using these statistics as the basis for judging the cavitation state. Liu et al. [60] analyzed the energy distribution characteristics of each wavelet coefficient of the centrifugal pump acoustic emission signal and concluded that the energy values in the frequency bands of 31.25–62.5 kHz, 62.5–125 kHz, and 125–250 kHz can be used to identify the cavitation state. Zhou et al. [86] conducted empirical mode decomposition (EMD) energy entropy analysis of the inlet pressure pulsation signals and obtained eigenvalues characterizing different cavitation states at the rated flow rate of the centrifugal pump. Similarly, Wang et al. [87] used the wavelet analysis method to perform a seven-layer wavelet decomposition of centrifugal pump inlet and outlet noise, extracting high-frequency and low-frequency information from different decomposition layers and analyzing their relative energy change rule. They also explored the time–frequency characteristics of centrifugal pump inlet and outlet cavitation noise. The analysis revealed that the development of cavitation significantly impacted the time–frequency characteristics of the centrifugal pump inlet and outlet noise, with slight differences in the frequency band influence. Specifically, in the inlet, the main frequency bands affected were 20–200 Hz, 250–1000 Hz, and 1500–2250 Hz, while in the outlet, the frequency bands were narrower, primarily affecting 20–200 Hz and 250–400 Hz, showing a trend of increasing, then decreasing, and then increasing.

6. Current Research Status of Cavitation State Identification Methods

Cavitation state identification involves classifying and categorizing samples into different types through the establishment of mathematical models. Signal analysis and feature extraction are essential in various cavitation states, providing a foundation for subsequent identification. The identification of the centrifugal pump cavitation state is achieved by acquiring, quantizing, and processing non-constant signals in different

cavitation stages. A set of data describing the cavitation characteristics is used, and statistical methods are employed to classify the cavitation features.

Wu [21] proposed a centrifugal pump cavitation state identification method that involves wavelet packet decomposition for noise reduction in vibration signals. The root mean square, energy entropy, and other eigenvalues of the eigenmatrix are extracted, and principal component analysis is used to normalize the matrix and reduce its dimensionality. The RBF neural network is utilized for cavitation state identification, and a software system is developed based on this method. Cao [67] introduced a cavitation identification method based on deep learning, constructing feature matrices from three sets of vibration signals. An automatic encoder based on deep learning is used for unsupervised learning of data features, achieving better identification results for the four types of cavitation states in centrifugal pumps compared to the BP neural network classification method. Song et al. [88] utilized EMD to decompose acoustic emission signals and obtain multiple intrinsic modal components, addressing the end-point problem and spurious modal problem in processing through the extreme value extension method and the correlation coefficient method. Zhou et al. [89] performed cavitation detection of hydraulic turbines using an acoustic emission detection technique and trained a BP neural network for identifying different states of cavitation. Jin [90] designed a pump system test and measurement system using LabVIEW for performance monitoring and data processing of centrifugal pumps. Fourier transforms and support vector machine methods were employed for cavitation identification, and a signal processing and identification interface was designed to achieve identification and prompt for primordial and severe cavitation phenomena in centrifugal pumps. Zhang [91] normalized the extracted eigenvalues as input sample eigenvectors and used Extreme Learning Machines (ELM) for the identification and classification of four types of centrifugal pump cavitation (no cavitation, cavitation incipient, critical cavitation, and severe cavitation). The ELM method accurately identified different cavitation states and outperformed the BP neural network method. Kumar et al. [92] proposed an algorithm for automatic signal processing, using various analytical methods to extract eigenvalues and continually adjusting the penalty factor of the support vector machine to enhance the accuracy of centrifugal pump fault identification.

7. Current Status of Cavitation Suppression Research

Currently, cavitation control methods in hydraulic machinery have emerged as a prominent area of interest within cavitation research. These methods can be broadly categorized into three main approaches: (1) mitigating cavitation occurrence by elevating the inlet pressure or incorporating induced wheels; (2) modifying the blade structure, such as introducing surface obstacles, slots, or holes; and (3) optimizing design parameters like the blade inlet angle of repose, blade outlet angle of repose, and blade wrapping angle [93]. These approaches hold significant promise for effectively managing cavitation-related issues and optimizing the performance of hydraulic machinery systems.

7.1. Increase Inlet Pressure

Starting with the root cause of cavitation, one effective approach to address this issue is to employ devices that can augment the inlet pressure, such as the induced wheel. The underlying principle is that when fluid flows through the induced wheel, vacuoles are generated at the outer edge of the wheel. The centrifugal force on the rim of the wheel squeezes these vacuoles, causing them to condense on the outer side of the induced wheel. As a result, the likelihood of cavitation occurring in the main impeller is significantly reduced. Several studies both domestically and internationally [94–97] have demonstrated that the installation of an induced wheel at the inlet can enhance the cavitation performance of centrifugal pumps. Additionally, incorporating jets at the inlet of centrifugal pumps has also shown promise in improving their cavitation performance. In both cases, the primary objective is to boost the pressure at the impeller inlet by externally introducing or increasing energy to suppress cavitation effectively.

7.2. Changing the Blade Structure

Cavitation suppression techniques involve modifying the blade structure by introducing obstacles, grooves, and holes on the blade surface. Xue [98] investigated the use of grooves on the back of axial pump blades, which effectively inhibited cavitation while enhancing the pump's external characteristics; rectangular grooves showed the best inhibition effect during incipient cavitation. Liu [99] employed a guide grid structure on the back of the blade, leading to effective cavitation inhibition at various flow rates and reduced blade deformation.

Xu [100] utilized a rough belt at the impeller back-cover plate and found that it enhanced pressure in certain flow field regions, altered vacuole morphology, and suppressed cavitation development. Selection of the specific speed ns = 32, speed n = 500 r/min of low specific speed centrifugal pump. Design parameters are: flow Q = 8.6 m^3/h, head H_0 = 4.2 m, impeller inlet diameter D_1 = 90 mm, impeller outlet diameter D_2 = 310 mm, impeller outlet width b_2 = 12 mm, blade inlet and outlet angle $\beta_1 = \beta 2 = 37^\circ$, the number of blades Z = 6. The rough belt layout in the impeller back covers 80~100% of the impeller diameter range, the height of its blade outlet width is 1/10, width of 1/4 blade thickness, and each impeller channel uniformly arranged 11, using the impeller back cover 80%~100% of the impeller diameter range, and its height of 1/10, width of 1/4 blade thickness. Its height is 1/10 of the width of the blade outlet, and its width is 1/4 of the thickness of the blade, and 11 of them are uniformly arranged in each impeller channel. The modified shear stress transport (SST) k-ω turbulence model is used, and the near-wall region is used in the k-ω turbulence model and the Kubota cavitation model. The dimensionless cavitation number is commonly used in fluid mechanics to describe the possibility and severity of the occurrence of cavitation, and Figure 12 shows the cavitation performance curve of the centrifugal pump. Figure 12 shows the cavitation performance curve of the centrifugal pump. From Figure 12, it can be seen that the numerical results of the centrifugal pump cavitation performance and the test comply with the better, while the error between the test value of the breaking head and the simulated value is less than 5.5%, which verifies the accuracy of the cavitation model. The conventional impeller breaking head is 2.55 m, while the rough belt structure of the impeller breaking head increased to 2.81 m, an increase of 10.2%. The results show that the arrangement of the rough belt can be a small improvement in the cavitation performance of the centrifugal pump impeller.

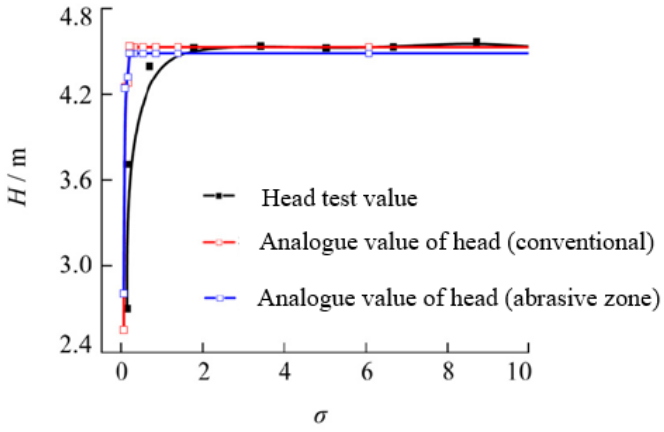


Figure 12. Centrifugal pump cavitation performance curve.

It can be seen from Figure 13a that with the change in the cavitation number, the pressure distribution of the cross-section in the impeller is significantly affected; in the stage of cavitation development, the low-pressure region in the impeller spreads to the outlet and is the main factor for the development of the cavitation in the centrifugal pump; the roughness band arranged at the outlet of the impeller rear cover plate increases the flow field pressure in the impeller, changes the outer morphology of the vacuole, and

achieves the inhibition of cavitation. The influence of the roughness band on the initial stage of cavitation is relatively small; in the stage of cavitation development, the existence of the structure effectively restricts the expansion of the low-pressure zone to the outlet, which increases the pressure at the outlet of the impeller, thus slowing down the process of cavitation, especially when the vacuole touches the position of the roughness band, while the high-pressure zone formed by the structure effectively prevents the development of the cavitation region to the outlet position. From Figure 13b, it can be seen that turbulent kinetic energy is concentrated in the impeller inlet and outlet regions, especially in the impeller channel in the region near the spacer tongue of the worm shell, which has a greater impact on the hydraulic and cavitation performance; with the gradual reduction of the cavitation number, the distribution region of high turbulent kinetic energy in the prototypical impeller is spreading from the impeller inlet to the impeller outlet gradually until the work stops in the impeller. The roughness zone reduces the turbulent kinetic energy in the impeller, especially in the position of the roughness zone, the turbulent kinetic energy intensity decreases more. The study shows that the roughness zone reduces the degree of energy dissipation and makes the flow more stable; the roughness zone shows a better inhibition effect in all stages of cavitation, and with the intensification of the degree of cavitation, its inhibition effect tends to be the largest. Figure 13c shows the equivalent surface of the volume fraction of vacuoles (α_v = 10%) and the flow line diagram of the impeller back cover. From Figure 13c, it can be seen that in the initial stage of cavitation, the roughness belt has no obvious effect on the vacuole morphology, but it can optimize the flow structure at the impeller outlet; in the stage of cavitation development, the roughness belt reduces the intensity of vortex in the impeller, especially for the impeller area near the tongue of the spacer, but the vacuole morphology has no obvious change; when the radial size of vacuole develops to the position of the roughness belt, the roughness belt changes the vacuole morphology at the same time and inhibits the vacuole effectively. This is because the rough zone can induce a large near-field pressure, forcing the vacuole morphology to partially change; in the severe stage of cavitation, the conventional structure impeller has completely lost the energy conversion ability, and the vacuole has filled the impeller channel, while the distribution range of the vacuole in the impeller with the rough zone structure is significantly reduced, and the energy exchange can be partially carried out in this state.

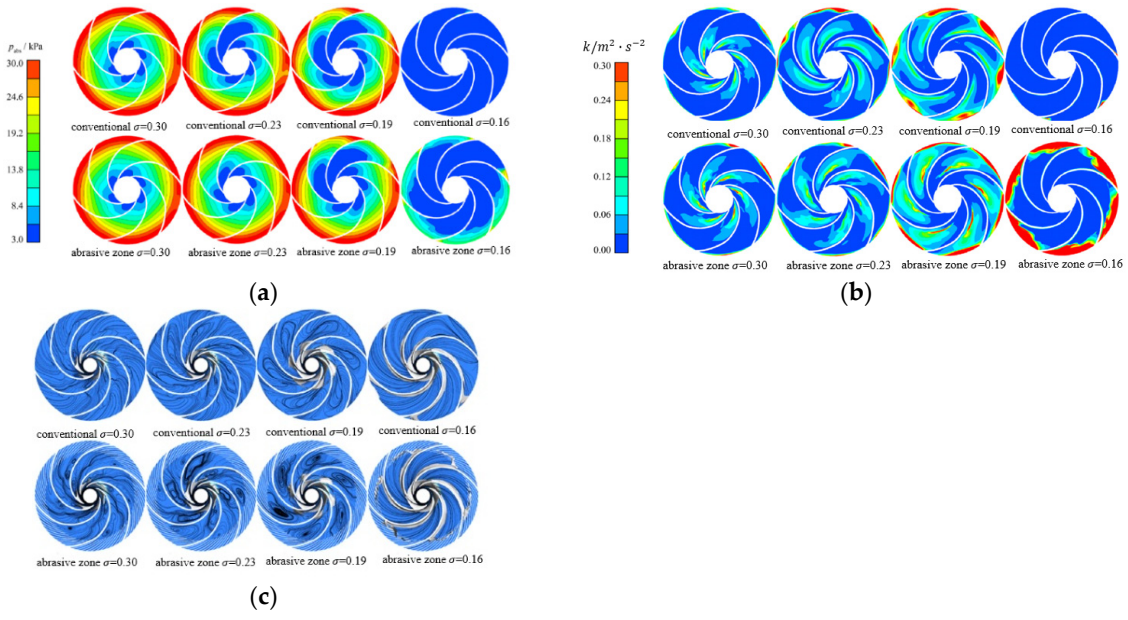


Figure 13. (**a**) Absolute pressure distribution in the middle section of the impeller, (**b**) turbulent kinetic energy distribution in the middle section of the impeller, and (**c**) vacuum bubble morphology and flow pattern [100].

Zhang [101] studied the impact of arranging spreading obstacles at different chord lengths on the blade cavitation performance and found that multiple spreading obstacles offered superior cavitation inhibition compared to a single obstacle. Zhao and others [49,102–106] focused on improving the cavitation performance of low-specific-speed centrifugal pumps by employing various methods, including blade surface obstacles, bypass devices, roughing the belt on the blade suction surface, small blades on the impeller back cover plate, and diversion blades. Introducing obstacles at 45% of the chord length on the centrifugal pump vane working surface demonstrated inhibiting effects on different cavitation phases. Additionally, the use of bypass piping in a specific type of centrifugal pump effectively inhibited the increase in vacuoles during the cavitation incipient and developmental periods, thereby enhancing the anti-cavitation performance of the centrifugal pump (Figure 14).

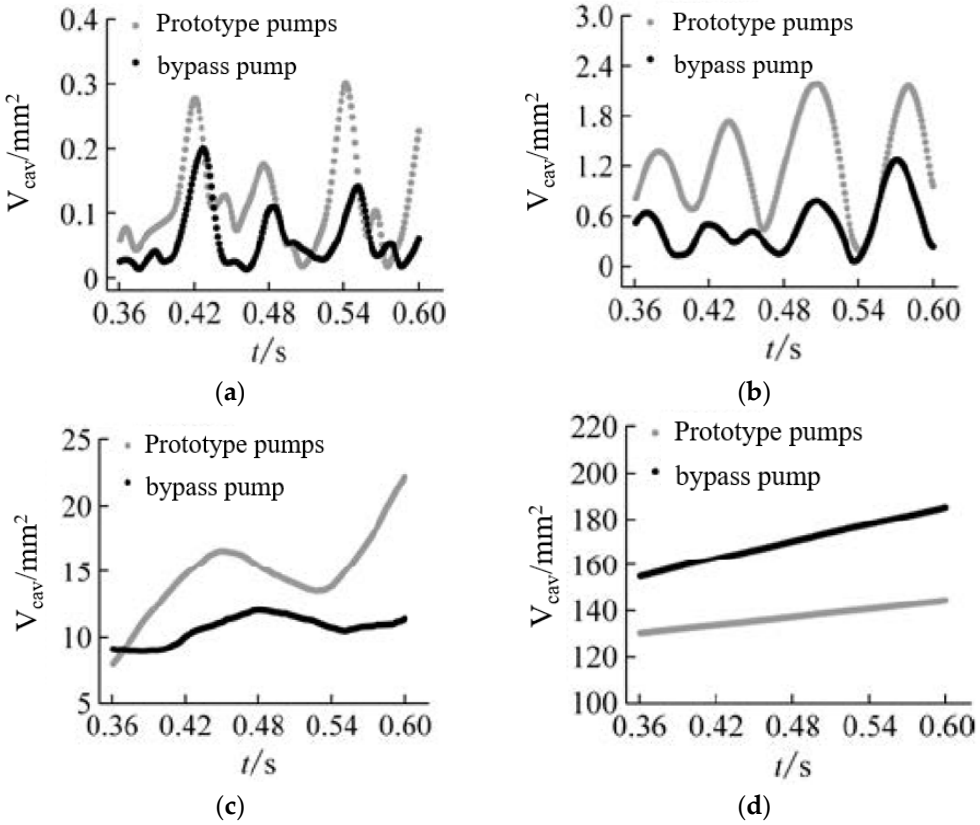


Figure 14. Plot of the change in the volume of the vacuole [102]: (**a**) σ = 0.84, (**b**) σ = 0.66, (**c**) σ = 0.30, and (**d**) σ = 0.13.

Liu et al. [107] observed that in low-flow conditions, vane grooving can alter the flow field structure, enhancing flow stability, and the optimal number of grooves exists to optimize overall performance. Similarly, Zhao and others [108] aimed to improve the cavitation performance of low-specific-speed centrifugal pumps by utilizing vane grooving and other methods to inhibit cavitation. Through numerical simulations, they analyzed the cavitation flow field structure and pressure pulsation characteristics at different cavitation stages. Hu et al. [109] investigated the impact of opening holes in the blade inlet on the impeller's cavitation performance. The study found that the through hole would cause energy loss in the impeller, and whether cavitation inhibition occurs in the centrifugal pump depends on the difference in pressure between the two sides of the vane and the magnitude of energy loss. Zhang et al. [110] improved the blade inlet side with a hole, and their study compared the centrifugal pump head and relative lift rate between unopened and different hole programs (Table 6). The locations and sizes of the blade holes (4 × 1 mm special hole program) are shown in Figure 15, and Figure 16 compares the cavitation situations of the

blades with unopened holes under different inlet pressures to the blades with a 1 mm hole at 0.01 MPa inlet pressure. The investigation focused on the effect of the hole size and arrangement on the cavitation performance of centrifugal pumps. Luo [111] considered five different slit schemes with varied position parameters at the leading edge of the vane. Numerical simulations of each scheme revealed that a suitable size of the slit structure at different positions on the vane's leading edge could enhance the cavitation performance of centrifugal pumps. The model with a position parameter α of 10% displayed optimal cavitation performance. Li [112] proposed a vortex control method based on the leading edge bionic convex junction, providing insights into the control mechanism's impact on the flow structure and cavitation morphology of the winding hydrofoil. The study confirmed that pressure pulsation primarily originates from cavity volume acceleration, and the bionic hydrofoil effectively suppressed cavitation by reducing pressure pulsation.

Table 6. Comparison of the centrifugal pump head and lift rate data relative to the unopened hole solution for different open hole solutions [110].

Programmatic	Lift/m	Upgrading Rate (%)
1 × 1 mm holes	43.85	1.39
1 × 2 mm holes	44.18	2.15
1 × 3 mm holes	44.75	3.47
4 × 1 mm holes	44.73	3.42

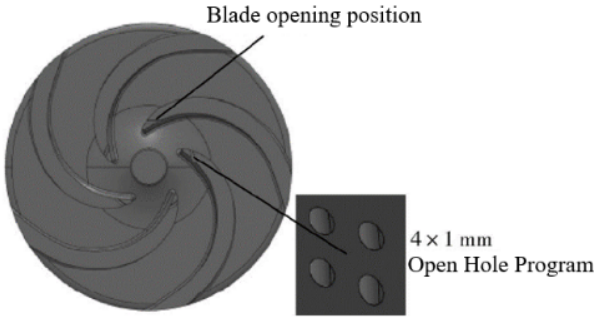


Figure 15. Blade aperture position and 4 × 1 mm special aperture scheme [110].

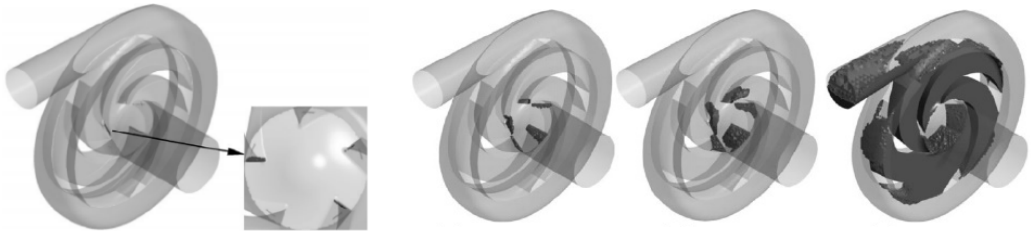


Figure 16. (**a**) Cavitation inside the open vane [110], and (**b**) internal cavitation under different inlet pressure conditions for unperforated blades [110].

7.3. Optimization of Design Parameters

Impeller parameter optimization, including vane top shape, vane number, vane placement angle, vane inlet impulse angle, and vane wrap angle, has shown promising results in enhancing cavitation resistance. Zhao et al. [113] focused on a flushing water propulsion axial pump and conducted simulations with different thicknesses and positions of the impeller's top. The study indicated that a strategically positioned top thickness could improve the pump cavitation performance and mitigate local cavitation occurrences. Wang and colleagues [114] optimized the shape of the vane inlet side, leading edge thickness, and

overall vane thickness for mixed-flow pumps. Their findings demonstrated that extending the vane inlet side in the appropriate direction, thinning the leading edge, and adjusting the blade thickness could significantly reduce the critical cavitation margin of mixed-flow pumps. Kang et al. [115] explored impeller import and export parameters and found that increasing the vane inlet placement angle enlarged the overflow area, thereby improving the cavitation performance of centrifugal pumps. The study revealed an optimal value for the impeller inlet parameters. Zhang and others [116] investigated the effects of various parameters on the cavitation performance of the induced wheel. Their results emphasized that the most influential factor in relation to the cavitation performance and hydraulic efficiency of the induced wheel is the inlet placement angle, followed by the inlet rounding wrap angle. Increasing the guide width of the induced wheel and the axial length of the blades also proved effective in enhancing cavitation performance. Yan and collaborators [117] optimized the cavitation characteristics of a cryogenic liquid nitrogen transfer pump by selecting the impeller inlet diameter, blade inlet angle of repose, and the number of blades as design variables. The study revealed that the blade inlet placement angle had the greatest impact on the cavitation performance. Post-optimization, the cryogenic pump exhibited a smaller critical cavitation margin, reduced cavitation region, and significantly improved overall cavitation performance. Liu and colleagues [118–120] investigated the effects of blade number, blade inlet impulse angle, and blade wrap angle on the required cavitation margin of centrifugal pumps with varying specific revolutions and verified their findings through experiments. The results highlighted the numerical simulation method's predictive accuracy, enabling an accurate understanding of the complex law of geometric parameter changes' influence on the centrifugal pump design flow and cavitation performance. Each parameter displayed an optimal value, optimizing the pump's cavitation performance, with the blade inlet impulse angle and blade wrap angle exhibiting a smaller influence compared to the number of blades. A comparison of the advantages and drawbacks of different cavitation suppression methods is shown in Table 7.

Table 7. Comparison of different cavitation suppression methods.

Cavitation Suppression Method	Steps	Advantages	Drawbacks
Increase inlet pressure	(1) Installation of guide wheels; (2) Incoming jet.	(1) Straightforward.	(1) Increased energy consumption; (2) System limiting pressure.
Changing the blade structure	(1) Arrangement of obstacles on the surface of the blade; (2) Slots and holes on the blade surface.	(1) Adjustment of blade structure to specific cavitation characteristics and flow conditions; (2) Direct, precise and efficient.	(1) Complex design; (2) Increase costs.
Optimization of design parameters	(1) Leaf apex shape, number of leaves; (2) Blade placement angle, inlet punching angle, blade wrapping angle.	(1) Comprehensive performance optimization; (2) A wide range of adaptability.	(1) Computationally intensive; (2) Running time.

8. Summary and Outlook

8.1. Research Summary

The research on the detection methods for centrifugal pump cavitation encompasses several approaches, including the flow-head method, high-speed photography method, pressure pulsation method, and predominantly, the acoustic and vibration methods. However, each method has its limitations, such as hysteresis, harsh conditions, or poor anti-interference. Among them, the acoustic and vibration methods have received more attention.

Regarding the extraction of the cavitation signal features of the centrifugal pump, the time-domain analysis provides direct access to the original signal but is susceptible

to interference and lacks reliability. On the other hand, the frequency-domain analysis assumes the signal to be relatively smooth, which is often not the case for dynamic signals with nonlinear and non-smooth characteristics. To comprehensively analyze the signal, time–frequency-domain analysis, and multi-dimensional feature extraction have gained prominence. Additionally, the varying operating conditions of centrifugal pumps pose a challenge as the cavitation feature frequency changes over time, necessitating the consideration of variable operating conditions during feature extraction.

In the domain of cavitation identification methods, various sensor-obtained signals undergo feature extraction to acquire corresponding cavitation state characteristics. Classifying different states of cavitation is achieved by processing and identifying the feature values using mathematical probability theory and statistical analysis on computers.

As for the study of cavitation inhibition methods, several strategies are explored, such as increasing the inlet pressure, incorporating induced wheels, introducing obstacles, slots, and holes on the blade surface, optimizing the blade structure, and adjusting design parameters like the blade inlet angle of repose, blade outlet angle of repose, and blade wrapping angle.

Overall, ongoing research in these areas continues to enhance the understanding of cavitation in centrifugal pumps, providing valuable insights into detection, feature extraction, identification, and inhibition methods for improved pump performance and reliability.

8.2. Research Outlook

Currently, the determination of the cavitation state in centrifugal pumps often involves combining numerical simulation and testing to analyze signal variations at different cavitation stages, extract relevant eigenvalues, and then apply pattern recognition techniques. Based on the methods discussed in this paper, further investigation and exploration can be pursued in the following areas:

(1) Diversified signal analysis methods can be employed to extract more comprehensive signal feature information. Techniques like wavelet analysis, envelope analysis, holographic spectral analysis, and others should be considered. Additionally, a variety of classification methods, such as genetic algorithms, particle swarm algorithms, artificial fish swarm algorithms, and others, could be explored. Utilizing multiple methods can strike a balance between recognition accuracy and efficiency.

(2) Improvements in cavitation state identification methods are crucial. Currently, signal processing of cavitation vibration noise in multi-measurement points often involves wavelet noise reduction, wavelet packet decomposition, statistical feature extraction, principal component analysis, radial basis function-based neural networks (RBF), and evidence theory (Dempster–Shafer) information fusion methods for identification. Further research should focus on other signal processing methods for signal separation and extraction, such as singular value decomposition noise reduction, Empirical Mode Decomposition (EMD) for eigenvalue extraction, and the use of support vector machines (SVM) for pattern recognition, aiming to enhance the cavitation state recognition accuracy.

(3) Regardless of whether it is centrifugal pumps or axial pumps, various cavitation states and stages exist, making accurate identification and classification, as well as real-time monitoring, crucial. Developing a new algorithm for recognizing and classifying images of different cavitation states, based on high-speed photography of these states, is essential. By creating a dataset and applying deep-learning methods for training, real-time monitoring and warning of different cavitation states can be achieved.

In conclusion, further research and exploration in these areas will contribute to advancing the understanding and detection of cavitation in pumps, leading to the improved performance and reliability of these critical engineering systems.

Author Contributions: Writing—original draft preparation, Y.Z. and L.Z.; writing—review and editing, S.L. and H.N.; visualization, X.L.; supervision, C.T. and Z.H.; project administration, Y.Z. and W.S.; funding acquisition, S.L. and W.S. All authors have read and agreed to the published version of the manuscript.

Funding: This research was funded by the Priority Academic Program Development of Jiangsu Higher Education Institutions (PAPD), Key R&D Projects of Jiangsu Province (grant number BE2023765), National Natural Science Foundation of China (grant numbers 51979138 and 52109106), Natural Science Foundation of Jiangsu Province (grant number BK20220609), Jiangsu Province Policy Guidance Program (International Science and Technology Cooperation) Project, Supported by the Open Research Subject of Key Laboratory of Fluid Machinery and Engineering (Xihua University), Sichuan Province (grant number LTDL-2022008, LTDL-2022001). Jiangsu Innovation Support Program (International Science and Technology Cooperation) Project (grant number BZ2023002).

Data Availability Statement: Data is contained within the article.

Conflicts of Interest: The authors declare no conflict of interest.

References

1. Zhang, K.W. *Principles of Fluid Mechanics. The First Book*; Machinery Industry Press: Beijing, China, 2000.
2. Kollek, W.; Kudźma, Z.; Stosiak, M.; Mackiewicz, J. Possibilities of diagnosing cavitation in hydraulic systems. *Arch. Civ. Mech. Eng.* **2007**, *7*, 61–73. [CrossRef]
3. Karpenko, M.; Stosiak, M.; Šukevičius, Š.; Skačkauskas, P.; Urbanowicz, K.; Deptuła, A. Hydrodynamic Processes in Angular Fitting Connections of a Transport Machine's Hydraulic Drive. *Machines* **2023**, *11*, 355. [CrossRef]
4. Savar, M.; Kozmar, H.; Sutlovic, I. Improving centrifugal pump efficiency by impeller trimming. *Desalination* **2009**, *249*, 654–659. [CrossRef]
5. Zhao, G.S. Research on Cavitation Flow Instability and Its Control in a Centrifugal Pump. Master's Thesis, Lanzhou University of Technology, Lanzhou, China, 2018.
6. Franc, J.P.; Michel, J.M. *Fundamentals of Cavitation*; Springer Science & Business Media: Berlin/Heidelberg, Germany, 2006. [CrossRef]
7. Bouziad, Y.A. Physical Modeling of Leading Edge Cavitation: Computational Methodologies and Application to Hydraulic Machinery. Ph.D. Dissertation, École Polytechnique Fédérale de Lausanne (EPFL), Lausanne, Switzerland, 2005.
8. Christopher, S.; Kumaraswamy, S. Identification of the critical net positive suction head from noise and vibration in a radial flow pump for different leading edge profiles of the vane. *ASME J. Fluids Eng.* **2013**, *135*, 121301. [CrossRef]
9. Hofmann, M.; Stoffel, B. Experimental and numerical studies in a centrifugal pump with two-dimensional curved blades in cavitating condition. *ASME J. Fluids Eng.* **2003**, *125*, 970–978. [CrossRef]
10. Li, X.J. Study on the Mechanism and Kinetic Characteristics of Non-Stationary Flow with Cavitation at the Leading Edge of a Centrifugal Pump Blade. Ph.D. Dissertation, Jiangsu University, Zhenjiang, China, 2013.
11. Bachert, B.; Ludwig, G.; Stoffel, B. Experimental investigations concerning erosive aggressiveness of cavitation in a radial test pump with the aid of adhesive copper films. In Proceedings of the Fifth International Symposium on Cavitation, Osaka, Japan, 1–4 November 2003.
12. Lu, J.X.; Yuan, S.Q.; Li, X.J.; Si, Q.R.; Luo, Y. Research on the characteristics of quasi-steady cavitation in a centrifugal pump. *IOP Conf. Ser. Mater. Sci. Eng.* **2015**, *72*, 032017. [CrossRef]
13. Tsujimoto, Y. Simple rules for cavitation instabilities in turbomachinery. In Proceedings of the Fourth International Symposium on Cavitation, Pasadena, CA, USA, 20–23 June 2001.
14. Kang, D.; Yonezawa, K.; Horiguchi, H.; Yutaka, K.; Yoshinobu, T. Cause of cavitation instabilities in three dimensional inducer. *Int. J. Fluid Mach. Syst.* **2009**, *2*, 206–214. [CrossRef]
15. Friedrichs, J.; Kosyna, G. Unsteady PIV flow field analysis of a centrifugal pump impeller under rotating cavitation. In Proceedings of the Fifth International Symposium on Cavitation, Osaka, Japan, 1–4 November 2003; pp. 8–12.
16. Pan, Z.Y.; Yuan, S.Q. *Fundamentals of Pump Cavitation*; Jiangsu University Press: Zhenjiang, China, 2013.
17. Ji, B.; Luo, X.W.; Wu, Y.L.; Peng, X.X.; Duan, Y.L. Numerical analysis of unsteady cavitating turbulent flow and shedding horse-shoe vortex structure around a twisted hydrofoil. *Int. J. Multiph. Flow* **2013**, *51*, 33–43. [CrossRef]
18. Roland, L.; Gerhard, R. Cavitation research at the Institute of Hydraulic Engineering and Water Resources Management. In Proceedings of the International Conference on Hydrodynamics, Wuxi, China, 30 October–3 November 1994; pp. 263–271.
19. Oba, R.; Ikohagi, T.; Yasu, S. Supercavitating Cavity Observations by Means of Laser Velocimeter. *J. Fluids Eng.* **1980**, *102*, 433. [CrossRef]
20. Hammitt, F.G. Cavitation Erosion: The State of the Art and Predicting Capability. *Appl. Mech. Rev.* **1979**, *32*, 665–675.
21. Wu, K. Research and Implementation of Centrifugal Pump Cavitation State Identification Method. Master's Thesis, Jiangsu University, Zhenjiang, China, 2019.

22. Escaler, X.; Egusquiza, E.; Farhat, M.; Avellan, F.; Coussirat, M. Detection of cavitation in hydraulic turbines. *Mech. Syst. Signal Process.* **2006**, *20*, 984–1007. [CrossRef]
23. Wang, J. Numerical Calculation and Experimental Research on Cavitation of the Hydraulic Device. Ph.D. Thesis, Jiangsu University, Zhenjiang, China, 2015.
24. Lu, X.J. Research on Design and Numerical Optimization of Middle-Open Multistage Centrifugal Pump. Master's Thesis, Jiangsu University, Zhenjiang, China, 2020. [CrossRef]
25. Wang, W.; Zhang, H.; Jiang, X.; Yang, X. A high-order and efficient numerical technique for the nonlocal neutron diffusion equation representing neutron transport in a nuclear reactor. *Ann. Nucl. Energy* **2024**, *195*, 110163. [CrossRef]
26. Zhou, Z.; Zhang, H.; Yang, X. H^1-norm error analysis of a robust ADI method on graded mesh for three-dimensional subdiffusion problems. *Numer. Algorithms* **2023**, 1–19. [CrossRef]
27. Zhang, H.; Liu, Y.; Yang, X. An efficient ADI difference scheme for the nonlocal evolution problem in three-dimensional space. *J. Appl. Math. Comput.* **2023**, *69*, 651–674. [CrossRef]
28. Tian, Q.; Yang, X.; Zhang, H.; Da, X. An implicit robust numerical scheme with graded meshes for the modified Burgers model with nonlocal dynamic properties. *Comput. Appl. Math.* **2023**, *42*, 246. [CrossRef]
29. Zhang, H.; Yang, X.; Tang, Q.; Xu, D. A robust error analysis of the OSC method for a multi-term fourth-order sub-diffusion equation. *Comput. Math. Appl.* **2022**, *109*, 180–190. [CrossRef]
30. Jiang, X.; Wang, J.; Wang, W.; Zhang, H. A Predictor–Corrector Compact Difference Scheme for a Nonlinear Fractional Differential Equation. *Fractal Fract.* **2023**, *7*, 521. [CrossRef]
31. Peng, X.; Ji, B.; Cao, Y.; Xu, L.; Zhang, G.; Luo, X.; Long, X. Combined experimental observation and numerical simulation of the cloud cavitation with U-type flow structures on hydrofoils. *Int. J. Multiph. Flow* **2016**, *79*, 10–22. [CrossRef]
32. Liu, H.L.; Wang, J.; Wang, Y.; Zhang, H.; Huang, H. Influence of the empirical coefficients of cavitation model on predicting cavitating flow in the centrifugal pump. *Int. J. Nav. Archit. Ocean Eng.* **2014**, *6*, 119–131. [CrossRef]
33. Ji, B.; Luo, X.W.; Arndt, R.E.A.; Peng, X.X.; Wu, Y.L. Large Eddy Simulation and theoretical investigations of the transient cavitating vortical flow structure around a NACA66 hydrofoil. *Int. J. Multiph. Flow* **2015**, *68*, 121–134. [CrossRef]
34. Singhal, A.K.; Athavale, M.M.; Li, H.; Jiang, Y. Mathematical Basis and Validation of the Full Cavitation Model. *J. Fluids Eng.* **2002**, *124*, 617–624. [CrossRef]
35. Schnerr, G.H.; Sauer, J. Physical and numerical modelling of unsteady cavitation dynamics. In Proceedings of the 4th International Conference on Multiphase Flow, New Orleans, LA, USA, 27 May–1 June 2001.
36. Zwart, P.J.; Gerber, A.G.; Belamri, T.A. Two-phase flow model for predicting cavitation dynamics. In Proceedings of the International Conference on Multiphase Flow, Yokohama, Japan, 30 May–3 June 2004.
37. Dorji, U.; Ghomashchi, R. Hydro turbine failure mechanisms: An overview. *Eng. Fail. Anal.* **2014**, *44*, 136–147. [CrossRef]
38. Xu, H.Q.; Shen, Z.P. Discussion of some problems in model cavitation and energy test of hydraulic turbine. *Water Resour. Hydropower Technol.* **1996**, *4*, 29–32.
39. Wu, D.; Wang, L.; Hao, Z.; Li, Z.; Bao, Z. Experimental study on hydrodynamic performance of a cavitating centrifugal pump during transient operation. *J. Mech. Sci. Technol.* **2010**, *24*, 575–582. [CrossRef]
40. Grekula, M.; Bark, G. Experimental Study of Cavitation in a Kaplan Model Turbine. *Minerva Anestesiol.* **2001**.
41. Wang, K.L. Research on Cavitation and Pressure Pulsation Characteristics of a Centrifugal Pump with High Specific Speed. Master's Thesis, Jiangsu University, Zhenjiang, China, 2020.
42. Cui, B.L.; Chen, J.; Li, X.J.; Lin, Z.; Cai, H.B.; Han, A.D. Visualization experiment and numerical simulation of cavitation development in high-speed induced wheel centrifugal pump. *J. Agric. Mach.* **2018**, *49*, 148–155.
43. Zhang, D.S.; Gu, Q.; Zhou, Q.; Huang, Y.D.; Shi, W.D. Experimental study of unsteady cavitation during startup of mixed-flow pump. *J. Vib. Shock* **2021**, *40*, 135–141. [CrossRef]
44. Zhang, D.S.; Gu, Q.; Chen, Z.H.; Shi, W.D. Numerical simulation and experimental study of transient cavitation characteristics during startup of a mixed-flow pump. In Proceedings of the 30th National Symposium on Hydrodynamics and the 15th National Symposium on Hydrodynamics, Hefei, China, 16–18 August 2019. [CrossRef]
45. Kim, J.; Song, S.J. Measurement of thermal parameter and Reynolds number effects on cavitation instability onset in a turbopump inducer. *J. Glob. Power Propuls. Soc.* **2017**, *1*, 157–170. [CrossRef]
46. Shen, X.; Zhang, D.S.; Liu, A.; Jin, Y.X.; Chen, J. Leakage vortex and vertical vortex cavitation characteristics of axial pump lobe top. *J. Agric. Eng.* **2018**, *34*, 87–94.
47. Sun, Z.X. Characterization of Cavitation-Induced Vibration Noise of Single Vane Centrifugal Pump. Master's Thesis, Jiangsu University, Zhenjiang, China, 2022. [CrossRef]
48. Guo, Z.W.; Pan, J.Y.; Qian, Z.D.; Cheng, Q. Cavitation performance test of axial flow pump with adjustable front guide vane. *J. Agric. Mach.* **2017**, *48*, 115–120+188.
49. Zhao, W.G.; Pan, X.W.; Lu, W.Q.; Xian, L.X. Unsteady cavitation characteristics of centrifugal pumps before and after perforation of vane inlet side. *J. Lanzhou Univ. Technol.* **2019**, *45*, 55–61.
50. Zhao, W.G.; Wang, G.P.; Zhao, G.S.; Xiao, T. Nonconstant cavitation flow characteristics of centrifugal pumps with low specific speed. *J. Lanzhou Univ. Sci. Technol.* **2020**, *46*, 50–56.
51. Wang, C.; Zhang, Y.X.; Ji, K.Z.; Xu, C.; Liu, M. Effect of cavitation on pressure pulsation in ultra-low specific rotation centrifugal pumps. *J. Agric. Mach.* **2020**, *51*, 122–129.

52. Mou, J.G.; Chen, Y.; Gu, Y.Q.; Zheng, S.H.; Qian, X. Characterization of fluid-solid coupling of centrifugal pumps under different cavitation degrees. *Vib. Shock* **2016**, *35*, 203–208. [CrossRef]
53. He, G.; Cao, Y.L.; Wang, S.C.; Ming, T.F.; Su, Y.S. Characterization of cavitation pressure pulsation in a centrifugal pump. *J. Wuhan Univ. Technol. (Transp. Sci. Eng. Ed.)* **2017**, *41*, 549–553.
54. Wang, K.L.; Li, H.; Shen, Z.H. Pressure pulsation characteristics of high specific rotation centrifugal pumps under cavitation. *J. Irrig. Drain. Mach. Eng.* **2020**, *38*, 891–897.
55. Wang, W.T.; Lu, H.; Wang, X. Transient cavitation flow pressure pulsation and vacuole morphology in a centrifugal pump. *China Rural. Water Conserv. Hydropower* **2017**, *9*, 202–206.
56. Yang, J.J.; Li, X.J.; Pan, Z.Y.; He, S. Influence of cavitation flow on pressure pulsation characteristics at the tongue of a double-wormed centrifugal pump. *J. Irrig. Drain. Mach. Eng.* **2020**, *38*, 445–450.
57. Lu, J.X. Research on Cavitation-Induced Non-Stationary Dynamic Characteristics of Centrifugal Pump and Its Mechanism. Ph.D. Thesis, Jiangsu University, Zhenjiang, China, 2017.
58. Lu, J.X.; Yuan, S.Q.; Siva, P.; Yuan, J.P.; Ren, X.D.; Zhou, B.L. The characteristics investigation under the unsteady cavitation condition in a centrifugal pump. *J. Mech. Sci. Technol.* **2017**, *31*, 1213–1222. [CrossRef]
59. Li, S.C. *Cavitation of Hydraulic Machinery*; Imperial College London Press: London, UK, 2000.
60. Liu, Z.; Zou, S.Y.; Li, Z.P.; Ju, W. Wavelet energy characterization of acoustic emission signals under centrifugal pump cavitation. *J. Agric. Eng.* **2015**, *31*, 99–103.
61. Dong, L.; Zhao, Y.Q.; Dai, C. Research on Cavitation Acoustic Characteristics of centrifugal Pump Based on Fluid-Acoustic field Coupling Method. *Adv. Mech. Eng.* **2018**, *10*, 1–13. [CrossRef]
62. Alfayez, L.; Mba, D. Detection of incipient cavitation and determination of the best efficiency point for centrifugal pumps using acoustic emission. *Proc. Inst. Mech. Eng. Part E J. Process Mech. Eng.* **2005**, *219*, 327–344. [CrossRef]
63. Su, Y.S.; Wang, Y.S.; Duan, X.Y. Research on the determination of cavitation monitoring threshold of the centrifugal pump. *J. Agric. Mach.* **2010**, *41*, 68–71.
64. Su, Y.S.; Wang, Y.S.; Yan, F.; Duan, X.Y. Modulation characterization and extraction method of cavitation vibration signal. *Vib. Test Diagn.* **2010**, *30*, 570–572. [CrossRef]
65. Zhao, Y.Q. Research on Centrifugal Pump Cavitation Judgment and Its Flow-Acoustic Characteristics. Master's Thesis, Jiangsu University, Zhenjiang, China, 2018.
66. Zeng, J.L. Experimental Study on Cavitation Vibration Noise Characteristics of the Centrifugal Pump. Master's Thesis, Lanzhou University of Technology, Lanzhou, China, 2015. [CrossRef]
67. Cao, Y.L.; Ming, T.F.; He, G.; Su, Y.S. Deep learning based cavitation state recognition of centrifugal pump. *J. Xi'an Jiao Tong Univ.* **2017**, *51*, 165–172.
68. Zhang, S.; Li, Z.H.; Liang, X.; Wei, X.B.; Xiao, B.Y. Characterization of centrifugal pump cavitation vibration based on SPWVD. *China Rural. Water Conserv. Hydropower* **2020**, *8*, 97–101.
69. Ye, Y.H.; Zhu, X.Y.; Sun, G.P.; Li, G.J. Evolution of vacuoles in centrifugal pumps and its effect on vibration. *J. Agric. Mach.* **2017**, *48*, 88–93.
70. He, G.; Cao, Y.L.; Ming, T.F.; Su, Y.S. Identification of centrifugal pump cavitation state based on improved octave band features. *J. Harbin Eng. Univ.* **2017**, *38*, 1263–1267+1302.
71. Ye, T.; Si, Q.R.; Shen, C.H.; Yang, S.; Yuan, S. Primary cavitation monitoring of centrifugal pumps based on support vector machine. *J. Irrig. Drain. Mach. Eng.* **2021**, *39*, 884–889.
72. Farhat, M.; Bourdon, P.; Gagné, J. Improving hydro turbine profitability by monitoring cavitation aggressiveness. In Proceedings of the CEA Electricity'99 Conference and Exposition, Vancouver, BC, Canada, March 1999; Available online: https://www.researchgate.net/publication/37424257 (accessed on 18 December 2023).
73. Yagi, Y.; Murase, M.; Sato, K.; Saito, Y. Preliminary study of detecting the occurrence of cavitation and evaluating TTS influence by an accelerometer mounted on a pipe. In Proceedings of the Fifth International Symposium on Cavitation, Osaka, Japan, 1–4 November 2003.
74. Cernetic, J. The use of noise and vibration signals for detecting cavitation in kinetic pumps. *Mech. Eng. Sci.* **2009**, *233*, 1645–1655. [CrossRef]
75. Tomaz, R.; Matevz, D.; Marko, H. An Investigation of the relationship between acoustic emission, vibration, noise, and cavitation structures on a Kaplan turbine. *ASME J. Fluids Eng.* **2007**, *129*, 1112–1122.
76. Lee, W.G.; Lee, J.W.; Hong, M.S.; Nam, S.H.; Jeon, Y.; Lee, M.G. Failure Diagnosis System for a Ball-Screw by Using Vibration Signals. *Shock Vib.* **2015**, *2015*, 435870. [CrossRef]
77. Buono, D.; Siano, D.; Frosina, E.; Senatore, A. Gerotor pump cavitation monitoring and fault diagnosis using vibration analysis through the employment of auto-regressive-moving-average technique. *Simul. Model. Pract. Theory* **2017**, *71*, 61–82. [CrossRef]
78. Zhou, Y.L. Research on Centrifugal Pump Cavitation State Identification Based on Improved Kernel Limit Learning Machine. Master's Thesis, Jiangsu University of Science and Technology, Zhenjiang, China, 2022. [CrossRef]
79. Li, X.J. Research on the Mechanism of Cavitation Non-Constant Flow at the Leading Edge of Centrifugal Pump Blade and Kinetic Characteristics. Ph.D. Thesis, Jiangsu University, Zhenjiang, China, 2013.
80. Duan, X.Y.; Wang, Y.S.; Su, Y.S. Application of vibration analysis in cavitation monitoring of centrifugal pumps. *Vib. Shock* **2011**, *30*, 161–165. [CrossRef]

81. He, Y.; Shen, Z. Formant-Based Ultrasonic Cavitation State Identifying Method, Involves Collecting Signal Data and Frame Data, and Determining Cavitation Area to Be not in Cavitation State When Base Frequency Average Value Is less than Ultrasonic Frequency: China, CN102590338-B. 16 April 2014. Available online: http://en.cnki.com.cn/Article_en/CJFDTOTAL-ZDCJ201216010.htm (accessed on 18 December 2023).
82. Qing, B.; Yu, B.; Lan, W.; Hu, J. Flow cavitation noise test of the centrifugal pump. *J. Drain. Irrig. Mach. Eng.* **2016**, *34*, 198–203.
83. Dong, L.; Xiao, J.W.; Ming, J.Y.; Liu, Y.L. Numerical simulation and experimental study on cavitation characteristics of hydraulic reducer model. *J. Irrig. Drain. Mach. Eng.* **2017**, *35*, 1–5.
84. Cudina, M. Detection of cavitation phenomenon in a centrifugal pump using audible sound. *Mech. Syst. Signal Process.* **2003**, *17*, 1335–1347. [CrossRef]
85. Wang, J.J.; Pan, L.P.; Cao, S.L. Application of wavelet transform to detection of cavitation signal in hydraulic turbine. *J. Hydropower Gener.* **2013**, *32*, 215–220.
86. Zhou, Y.L.; Liu, Y.Q.; Xue, G.X.; Chen, J. Centrifugal pump cavitation fault diagnosis based on EMD and marginal spectral band energy. *J. Chem. Eng.* **2012**, *63*, 545–550.
87. Wang, D.W. Research on Cavitation Acoustic Response Characteristics and Cavitation Suppression Method of Centrifugal Pump. Ph.D. Thesis, Lanzhou University of Science and Technology, Lanzhou, China, 2022. [CrossRef]
88. Song, J.C. EMD-Based Signal Processing Method of Cavitation Acoustic Emission from Hydraulic Turbine. Master's Thesis, Changsha University of Science and Technology, Changsha, China, 2017.
89. Zhou, Y.G. Feature Extraction and State Identification of Cavitation Acoustic Emission Signal of Hydraulic Turbine. Master's Thesis, Changsha University of Science and Technology, Changsha, China, 2019. [CrossRef]
90. Jin, L.C. Hydrodynamic Noise Signal Analysis and Cavitation Identification of Single Vane Centrifugal Pump Based on Support Vector Machine. Master's Thesis, Jiangsu University, Zhenjiang, China, 2021. [CrossRef]
91. Zhang, X.Y. Feature Extraction and State Identification of Cavitation Acoustic Emission Signal of the Centrifugal Pump. Master's Thesis, Changsha University of Science and Technology, Changsha, China, 2020. [CrossRef]
92. Kumar, A.; Kumar, R. Time-frequency analysis and support vector machine in automatic detection of defect from vibration signal of the centrifugal pump. *Measurement* **2017**, *108*, 119–133. [CrossRef]
93. Shen, Z.H. Study on the Cavitation Characteristics of High Specific Speed Pump with Small Flow Rate and Optimization of Cavitation Performance. Ph.D. Thesis, Jiangsu University, Zhenjiang, China, 2021. [CrossRef]
94. Han, W.; Zheng, H.; Wang, L.Q.; Zhang, Z.Z.; Su, M. Analysis of the effect of staggered vane arrangement on cavitation performance of double-suction pump. *J. Agric. Mach.* **2017**, *48*, 124–131+140.
95. Deng, Y.X.; Li, R.N.; Han, W.; Yang, W.J.; Li, Z.G. Cavitation characteristics of return vortex in a spiral centrifugal pump. *J. Agric. Eng.* **2015**, *31*, 86–90.
96. Agostino, L.; Torre, L.; Pasini, A. On the preliminary design and non cavitating performance prediction of tapered axial inducers. *J. Fluids Eng.* **2008**, *130*, 119–120.
97. Okita, K.; Ugajin, H.; Matsumoto, Y. Numerical analysis of the influence of the tip clearance flow on the unsteady cavitating flows in a three-dimensional inducer. *J. Hydrodyn.* **2009**, *21*, 34–40. [CrossRef]
98. Xue, Z.Y. Study on the Effect of the Slotted Vane on Cavitation Performance of Axial Flow Pump. Master's Thesis, Lanzhou University of Science and Technology, Lanzhou, China, 2021. [CrossRef]
99. Liu, Y.L. Influence of Vane Guide Grille on Cavitation and Fluid-Solid Coupling Characteristics of Axial Pump. Master's Thesis, Xi'an University of Technology, Xi'an, China, 2021. [CrossRef]
100. Xu, Z.X. Study on the Cavitation Inhibition Effect of the Roughness Zone on the Impeller Rear Cover of the Centrifugal Pump. Master's Thesis, Lanzhou University of Science and Technology, Lanzhou, China, 2020. [CrossRef]
101. Zhang, C.L. Research on the Inhibition of Cavitation of Axial Flow Pump by Obstacles. Master's Thesis, Lanzhou University of Science and Technology, Lanzhou, China, 2022. [CrossRef]
102. Zhao, W.G.; Zhu, C.J.; Xu, Z.X.; Xu, Y. Numerical simulation and test of the cavitation characteristics of centrifugal pump controlled by bypass device. *Vib. Shock* **2021**, *40*, 119–126. [CrossRef]
103. Zhao, W.G.; Li, Q.H.; Kang, Y.D. Study on the cavitation inhibition effect of suction surface roughness zone of centrifugal pump blade. *J. Agric. Mach.* **2021**, *52*, 169–176+214.
104. Zhao, W.G.; Pan, X.W.; Song, Q.C.; Li, S.S. Effect of vane inlet side perforation on the cavitation performance of centrifugal pumps. *J. Irrig. Drain. Mach. Eng.* **2019**, *37*, 461–469.
105. Zhao, W.G.; Xian, L.X.; Zhao, G.S.; Pan, X.W. Numerical prediction of the effect of diverter vanes on the cavitation performance of centrifugal pump. *J. Lanzhou Univ. Technol.* **2019**, *45*, 56–62.
106. Zhao, W.G.; Zhao, G.S.; Xian, L.X.; Han, X.D. Numerical simulation and experiment on inhibiting cavitation by arranging obstacles on the blade surface of the centrifugal pump. *J. Agric. Mach.* **2017**, *48*, 111–120.
107. Liu, W.; Yuan, S.Q.; Li, X.J.; Pan, Z.Y. Influence of vane grooving on the internal flow of a low specific rotation centrifugal pump. *J. Irrig. Drain. Mach. Eng.* **2013**, *31*, 11–14.
108. Zhao, W.G.; Zhai, L.J.; Xia, T.; Li, S.S. Numerical simulation of centrifugal pump blade grooving to inhibit cavitation. *J. Agric. Mach.* **2018**, *49*, 150–157.
109. Hu, Z.A.; Wang, J.X.; Zhu, B.S.; Liu, X.B. Effect of centrifugal pump impeller perforation on cavitation performance. *Therm. Power Eng.* **2018**, *33*, 44–51. [CrossRef]

110. Zhang, J.; Chen, X.P.; Su, C.M.; Zhao, Z. Study on the effect of vane inlet side opening on cavitation and turbulent energy in centrifugal pumps. *Fluid Mach.* **2021**, *49*, 14–19. [CrossRef]
111. Luo, Y.X. Research on the Effect of Leading Edge Open Slit Vane on the Cavitation Performance of Centrifugal Pump. Master's Thesis, Lanzhou University of Science and Technology, Lanzhou, China, 2022. [CrossRef]
112. Li, J. Scale Analysis of Non-Constant Cavitation Flow and Bionic Control Mechanism of Winding Blade. Ph.D. Thesis, Jilin University, Changchun, China, 2022. [CrossRef]
113. Zhao, C.S.; Li, C.; Li, P.Z. Influence of blade thickness on cavitation performance of water jet propulsion axial pump. *Mar. Eng.* **2021**, *43*, 61–66. [CrossRef]
114. Wang, W.; Lu, P.B.; Wang, X.F.; Qin, G.X.; Wang, Y.M. Optimization of mixing pump blades and cavitation study based on equation of state model. *J. Dalian Univ. Technol.* **2013**, *53*, 29–35.
115. Kang, J.Y.; Zhu, R.S.; Wang, X.L.; Liu, Y.; Zhong, W.Y. Influence of impeller geometry parameters on fracture cavitation performance of centrifugal pumps. *J. Irrig. Drain. Mach. Eng.* **2018**, *36*, 111–117.
116. Zhang, Y.T.; Chen, H.; Xiang, L.; Chen, W.; Xu, K.F. Study on cavitation performance of induced wheel based on orthogonal optimization design. *Propuls. Technol.* **2020**, *41*, 343–352. [CrossRef]
117. Yan, Z.C.; Shao, C.L. Optimized design of cavitation performance of cryogenic pump based on orthogonal test. *Petrochem. Equip.* **2019**, *48*, 1–7.
118. Wang, Y.; Liu, H.L.; Liu, D.X.; Wang, J.; Wu, X.F. Influence of vane wrap angle on flow-induced vibration noise of centrifugal pump. *J. Agric. Eng.* **2013**, *29*, 72–77.
119. Wang, Y.; Liu, H.L.; Yuan, S.Q.; Liu, D.X.; Wang, J. Cavitation vibration and noise characteristics of centrifugal pumps with different vane package angles. *J. Irrig. Drain. Mach. Eng.* **2013**, *31*, 390–393.
120. Tan, M.G.; Wang, Y.; Liu, H.L.; Wu, X.F.; Wang, K. Influence of vane number on internal flow-induced vibration noise of centrifugal pump. *J. Irrig. Drain. Mach. Eng.* **2012**, *30*, 131–135.

Disclaimer/Publisher's Note: The statements, opinions and data contained in all publications are solely those of the individual author(s) and contributor(s) and not of MDPI and/or the editor(s). MDPI and/or the editor(s) disclaim responsibility for any injury to people or property resulting from any ideas, methods, instructions or products referred to in the content.